THE GEOPHYSICAL INSTITUTE OF ISRAEL המכון הגיאופיסי לישראל
P.O.B. 182, LOD 71100, ISRAEL, TEL: 972-8-9785888, FAX: 972-8-9208811 - רח' הבעש"ט 6, לוד
www.gii.co.il

SEDIMENT AMPLIFICATION FROM AMBIENT NOISE EXCITATION IN THE SOUTHERN PART OF THE ZEVULUN PLAIN: A TOOL FOR RECONSTRUCTION SUBSURFACE STRUCTURE

December, 2007 **Report No 503/292/07**

Principal Investigator:

Dr. Y. Zaslavsky

Collaborators:

T. Aksinenko, M. Gorstein, M. Kalmanovich, D. Giller, I. Dan, N. Perelman, G. Ataev, V. Giller, I. Livshits, and A. Shvartsburg

Prepared for
The Steering Committee for
National Earthquake Preparedness

TABLE OF CONTENTS

LIST OF FIGURES

LIST OF TABLES

ABSTRACT

Horizontal-to-vertical (H/V) spectral ratios from a single ambient noise record are used to define the thickness of sedimentary layers in the context of seismic hazard assessment and identification of the faults. At the request of the Geological Survey of Israel the Seismology Division, Geophysical Institute of Israel, carried out a series of ambient noise measurements along four SN directed profiles located in the southern part of the Zevulun plain. Total length of profiles is 17.5 km and 76 sites (instead of planned 50 sites) were instrumented for varying periods of time.

In our study we use the shear wave structures for different sediments obtained in the earlier studies. Fixing the shear wave velocity, it is possible to adjust the thickness of sedimentary layers for matching analytical response functions with experimental spectral ratios.

Our investigation demonstrates that the H/V curves exhibit two clear peaks appearing at different frequencies. Our recent studies (see e.g Zaslavsky et al., 2006) show that such an observation is associated with two impedance contrast: one at deeper and other at shallow strata. The corresponding frequencies are interpreted as fundamental (f_0), and other natural (f_1) ones. Similar conditions are observed in most of analyzed sites

Change of shape of the H/V spectral ratios allows differentiating reflectors which change over the entire area. Frequencies of the first and second peaks in the H/V spectral ratios are used to define the thickness of sediments to reconstruct multi-layer 1-D models.

Sites, where sharp changes in the fundamental frequency and/or change in the shape of the H/V ratio over a short distance are observed, are identified as fault. In some cases the faults defined as a result of geological interpretation of ambient noise measurements, do not coincide with existing geological representations.

Our results suggest that measurements of ambient noise solely along profiles in the area, where detailed microzonation study has not previously performed, may hamper interpretation of results and affect their fidelity and stability. Microtremor survey with dense grid of measuring sites over the study area facilitates constructing the cross sections, tracing faults and developing maps of depth of a reflector.

1. INTRODUCTION

Dead Sea Fault has been continuously active and was the source of several destructive earthquakes that shook the entire region throughout geological times (Amiran et al., 1994; Begin, 2005). Over the past two centuries, large earthquakes with intensities reaching X on the MM scale occurred in the area. The earthquake of October 30, 1759, (Amiran at al., 1994), located probably in southern Lebanon, affected most of today Lebanon, Israel and Syria with damages extended as south as Jaffa. Some sources report a death toll of 10,000-40,000 people. According to Ambraseys and Barazangi (1989) losses were certainly considerable. The earthquake that occurred on January 1, 1837, was the strongest earthquake to occur in the region since the 19-th century (Amiran et al., 1994), were most of the damage is reported to occur in Safed and Tiberias. The July 11, 1927, earthquake, with magnitude M=6.2, was the most destructive regional seismic event in the 20-th century. The effects of the earthquake were devastating, particularly in Jerusalem and in the towns of Lod and Ramle. In Lod and Ramle, which at that time were small towns, many buildings were destroyed and 50 people were killed (Avni et al., 2002). We note that these towns are relatively distant from the epicentre, i.e., about 60 km. In the earthquake of January 749 with possibly a similar magnitude the flourishing Roman-Byzantine town of Bet Shean was destroyed.

The amplification of ground motion from earthquakes due to local geology is a great importance in earthquake hazard and risk evaluations. Site effects associated with ground motion amplification at resonance frequency of a building may have severe consequences. In the last decade, the Geophysical Institute of Israel has launched a number of projects to identify and map areas which are expected to amplify seismic ground motions across Israel (i.e., Zaslavsky et al., 1995, 2000, 2003, 2005a,b, 2007a; Shapira et al., 2001). Site specific hazard assessment in urban areas requires additional studies focussing on modelling and characterization of the subsurface at different locations within the study area. In order to evaluate site effects analytically, S-wave velocity structure of the unconsolidated sediments and S-wave contrast between reflectors and sediments should be properly determined.

The S-wave velocity structure can be obtained through active in-situ measurements using horizontally oriented sources or downhole and crosshole techniques. However, these methods are expensive and slow and often cannot be used in urban areas. In recent years different studies

show that the resonance frequency of the site obtained from horizontal-to-vertical spectral ratios of ambient vibration can be used to estimate average shear velocity structure and to map of thickness of soft sediments (Ibs-von Seht and Wohlenberg, 1999; Fäh, at al., 2000; Kobayashi et al., 2000; Delgado et al., 2000; Parolai et al., 2002; Hinzen et al., 2004; D'amico et al., 2004; Zaslavsky et al., 2007b). However, the function describing the average velocity versus depth for the sedimentary cover of the basin is derived under assumption of lateral homogeneity and smooth vertical variations of velocity due to different lithological units in layered media. Our investigations in different areas of Israel (Zaslavsky et al., 2004, 2005c, 2006b) showed that general relationship between fundamental frequency and depth of reflector does not deliver an accurate estimate of the local sediment thickness and cannot be used for hard-rock basement mapping.

Many authors assume ambient noise is primarily composed of surface wave (Lachet and Bard, 1994; Conno and Ohmatchi, 1998; Arai and Tokimatsu, 2004). Consequently, the comparison of H/V ratio from ambient noise with the transfer function of S waves is problematic. Others such as Nakamura (2000), Zhao et al. (2000), Enomoto et al. (2000) and Mucciarelli and Gallipoli (2004) claim that the H/V spectrum of ambient noise is dominated by the upward propagation of SH wave through the layered media. Whoever is right, both models agree that the H/V spectra and the site response function for SH wave are the results of the velocity structure of the media, that both exhibit the same fundamental resonance frequencies with similar amplitudes at least when considering small motions. The authors of this study demonstrated, through many previous studies when noise measurements were made near boreholes and/or near refraction surveys, that the fundamental frequency and its corresponding H/V amplitude derived from the analysis of ambient noise are practically the same as the fundamental frequency and its corresponding amplification level derived from the computed transfer function of SH waves at low strains propagating through a relatively simple 1-D model of the site, known from geo-technical and geophysical surveying. Therefore, in order to construct models of the subsurface, we may start at sites close to refraction lines and bore-holes, where we have subsurface information.

The aims of this study is to obtain a better knowledge of the structure in the southern part of the Zevulun plane by using the horizontal-to-vertical spectral ratio from ambient noise measured closely spaced (250 m) stations across four profiles, detailed comparison of the

analytical and experimental site response functions, reconstruction the subsurface structure and to construct geological cross-section

2. GEOLOGICAL FRAMEWORK

The geological map in Fig. 1 shows location of the measuring sites along profiles 1, 2, 3, 4. Profiles cross the southeastern part of the Qishon Graben in the S-N direction. Geological data used in the present study are collected from several sources. In particular, depth of the Top Judea Gr. is compiled from the structural maps of Mero (1983) and Fleisher and Gafsou (2003), and also a study of Bar Yossef et al. (2003). Borehole information and geological cross sections across the study area (Kafri and Ecker, 1964) are used to determine general subsurface conditions, local site stratigraphy and composition of the soils. The general geology is taken from the Geological Map of Israel (1998). The geology of the shelf and continental margin offshore Haifa is largely described by Almagor and Hall (1980), Almagor (1993) and Eytam et al. (1992).

The geological structure of the study area is rather complex. It explains considerable differences in definition of faults locations by Fleischer and Gafsou (2003) and by Mero (1983) (see Fig. 1).

The Qishon Graben came to existence during the Eocene. The deposition of Qishon Graben formations was governed by tectonic activity and sea level fluctuations causing transgressions and regressions. Two main phases of tectonic activity can be recognized in the Zevulun Plain.

An early Neogene phase of block faulting created the Qishon Graben. During the Miocene this graben was filled by calcareous sediments, by considerable thickness of conglomerates and by some evaporates. The Pliocene transgression was limited to the depression of the Qishon Graben, where a thick complex of clays and marls was deposited. The second phase of tectonic activity was during the late Pliocene - Early Pleistocene resulting in a phase of uplift and faulting, accompanied by volcanic activity. As a result, the Qishon graben was deepened.

The main stratigraphic units of the sedimentary column in the study area are the Judea, Mt. Scopus, Avedat, Saqiye and Kurkar Groups (compiled from Mero, 1983; and Kafri, 1964).

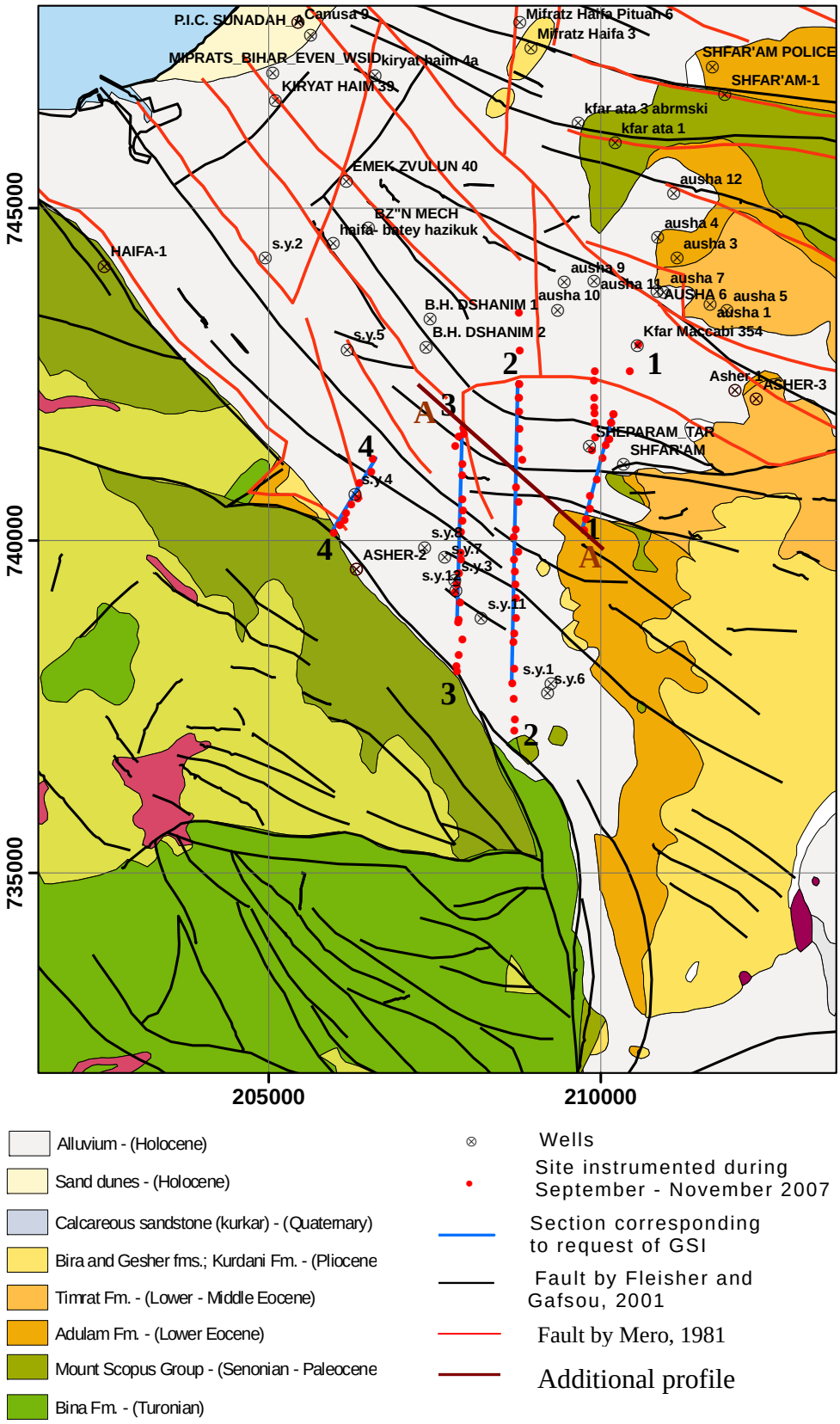

Figure 1. Geological map and location of measuring sites

The Judea Gr. of Cenomanian- Turonian age is represented mainly by the dolomites and limestones. Its depth of bedding in the investigated area varies from several meters near the Carmel Fault to 700-800 meters at centre of the Graben (Fleisher and Gafsou, 2003).

The Mount Scopus Gr**.** is overlying the Judea Gr., and is composed of Senonian to Paleocene formations, which are represented by chalk and marls, sometimes bituminous. The Avedat Group of Eocene age is composed of the Zor'a and Timrat Formations and is represented by chalk and chalky limestone. Zor'a Formation is subdivided into two members: Adulam and Maresha. Adulam Member overlies the Mount Scopus Gr. conformably and crops out over the eastern part of the study area. The northern part of profile 1 is located on the outcropping Adulam Member.

The Saqiye Group overlies the Mt. Scopus and Avedat Groups uncomformably and is overlain by the Kurkar Group. The Saqiye Group is composed of the Bet Guvrin (Upper Eocene - Early Miocene), Lakhish (Oligocene - Early Miocene), Ziqlag and Mavkiim (Upper Miocene) and Yafo (Upper Miocene to Pliocene) Formations. Bet Guvrin and Lakhish Formations are represented by chalk and marl with intercalations of limestone layers. Ziqlag Formation is represented by bioclastic, reefal limestone with intercalations of marl and chalk. Lithology of Mavkiim Formation is massive layers of anhydrite. Yafo Formation is represented mainly by clays and marls of marine and continental origin.

The Kurkar Group consists of the Pliocene and Pleistocene age formations. Kurdane Formation of Upper Pliocene - Lower Pleistocene age is represented by sandy limestone to calcareous limestone, rich in fossils, shells and algae. Deposits of the Kurdane Formation are found only in the eastern part of the Qishon Graben.

A number of marine transgressions of the Quaternary epoch produced a sequence of interbedded strata of dune sands and lagoonal clays in the subsiding graben structure. The general lateral variation of sediments in the Qishon Graben from NW to SE shows the following pattern:

- marine clays and silts in the western part of the graben;
- eastwards, marine and littoral calcareous sands as beach barriers and dune formations These sand strata are commonly partly cemented and known as Kurkar;

- mainly lagoonal clays, silts and loams in the eastern part of the graben, developed behind the coastal dune formations.

From our experience and knowledge, accumulated from the former studies carried out in the Zevulun Plain (2006 and 2007), we suppose the following lithostratigraphic units to be potential reflectors owing to their geotechnical characteristics:

- Top Judea Gr. is identified as the deepest reflector;
- Top Mount Scopus Gr. or top Avedat Gr., which have close velocity characteristics, we presume as a shallow reflector in the southeastern part of studied area;
- Top Mavkiim or Ziqlag Formation we presume as deep reflector in that part of graben, where Top Judea Gr. is so deep, that cannot serve as a reflector any more: and as a shallow reflector, while Top Judea Gr. is fundamental one;
- The impedance contract between sand/sandy loam and calcareous sandstone the Kurkar Gr. or clay of Yafo Fm. may cause additional reflection that we have already fixed in our former investigations.

3. AMBIENT NOISE MEASUREMENTS AND ANALYSIS

Ambient noise measurements along four profiles were carried out by request of the Geological Survey of Israel during the period September to November 2007. Total length of lines is 17.5 km and 76 sites (instead of planned 50 sites) are instrumented for varying periods of time. The distribution of measurements points over the study area is shown in Figure 1. Ambient noise measurements are conducted using portable instruments (Shapira and Avirav, 1995) consisting of a multi channel amplifier, Global Positioning System (GPS) and a laptop computer with 16-bit analog-to-digital conversion card. Each seismograph station consists of three (one vertical and two horizontal) L4C velocity transducers (Mark Products) with a natural frequency of 1.0 Hz and damping ratio 70% of critical. The recorded signals are sampled at 100 samples per second and band-pass filtered between 0.2 Hz and 25 Hz.

Prior to performing measurements, the individual seismometer constant (free-frequency, damping and motor constant) are determined using sine and step calibration signals, and then the frequency response function of all channels are computed. As a final test, all seismometers are placed at the same location and in the same orientation to record the same waves.

As already observed by many researchers, there is a high scatter in the H/V spectra. The source of the scatter is debated between the researchers. Mucciarelli (1998), for example, claims that traffic is not a major reason, whereas Horice et al. (2001) used in their analysis recordings of microtremor originated by passing traffic. Recently, Parolai and Galiana-Merino (2006) showed that influence of transients on the H/V spectral ratio is insignificant. Our observations also indicate that the effect of transients is almost unnoticeable. In order to reduce the scatter and increase stability, our processing scheme involves a careful selection of the time windows from which we obtain H/V functions. It follows the concept that at site with no site effects the amplitude spectra of the H and V components of the ground motions are of the same level throughout the spectrum. At sites with significant site effects, the spectral amplitudes of the two components differs only within a certain limited frequency band, probably at the neighbourhood of the resonance frequency. Time windows that exhibit such or similar conditions are selected. The selection was made manually and yields an appreciated deduction in the H/V scatter. Continuous record of ambient noise for 60-70 minutes enables to select sufficient number of suitable samples for analysis.

For each site we determine the average H/V spectral ratios and their corresponding standard deviations by applying the following process: time windows, each of 30 sec long, provide sets of H and V ground motions that are Fourier transformed using cosine-tapering (1 sec at each end) before transformation. The spectra are then smoothed with a triangular moving Hanning window. More precisely, we apply “window closing” procedure (see Jenkins and Wats, 1968) for smart smoothing of spectral estimates so that any significant spectral peaks are not distorted. For each site we compile a set of up to 50 selected time windows, each window providing an H/V spectral function.

The average spectral ratio for each of two horizontal components is computed; if the curves of average spectral ratios of the two components are similar then the average of the two horizontal-to-vertical ratios is defined as:

$$A(f) = \frac{1}{2n}\left[\sum_{i=1}^{n}\frac{S_{NS}(f)_i}{S_V(f)_i} + \sum_{i=1}^{n}\frac{S_{EW}(f)_i}{S_V(f)_i}\right] \qquad (1)$$

Where $S_{NS}(f)_i$ and $S_{EW}(f)_i$ are individual spectra of the horizontal components and $S_V(f)_i$ is individual spectrum of the vertical component.

Coordinates of the measurements points, the fundamental (f_0) and natural (f_1) frequencies and their associated H/V levels are shown in Table 1.

Table 1. Coordinates of the measurement points, H/V resonance frequencies and their associated amplitude levels.

No.	Point	Profile	Coordinates		Results			
			EW	*NS*	f_0 (Hz)	Amplitude	f_1 (Hz)	Amplitude
1	**2**	**3**	***4***	***5***	**6**	**7**	**8**	**9**
1	1	1	209744	740174	1.25	2.30		
2	2	1	209770	740350	1.20	2.10	8.00	2.60
3	3	1	209832	740504	0.62	2.10	2.20	4.50
4	4	1	209832	740689	0.65	2.10	2.20	4.40
5	5	1	209935	740943	0.50	2.50	2.15	4.40
6	6	1	210021	741260	0.50	2.20	2.00	6.50
7	7	1	210120	741548	0. 80	2.40	1.35	4.20
8	7A	1	210120	741548	0. 80	2.40	1.35	4.20
9	8	1	210151	741791	0.75	2.10	1.40	4.40
10	8A	1	210151	741791	0.75	2.10	1.40	4.40
11	9	1	210185	741930	0.50	2.00	1.60	4.60
12	9A	1	210185	741930	0.50	2.00	1.60	4.60
13	10	2	208765	742373	0.45	3.00	1.15	3.50
14	10A	2	208765	742373	1.10	4.00	1.90	2.50
15	11	2	208762	742165	1.00	4.00	1.90	3.00
16	11A	2	208762	742165	1.00	4.00	1.90	3.00
17	12	2	208766	741958	0.90	4.30	1.60	3.00
18	13	2	208767	741702	0.95	3.90	1.70	3.00
19	14	2	208760	741403	0.90	3.50	1.65	2.20
20	15	2	208811	741241	0.85	3.60	1.40	3.00
21	16	2	208716	740820	1.20	3.25		
22	17	2	208756	740607	0.6	2.3	1.6	3.4
23	18	2	208712	740181	0.60	2.50	2.60	3.50
24	19	2	208682	740066	0.60	2.40	2.45	5.70
25	20	2	208752	739858	0.60	2.00	2.40	4.85
26	21	2	208685	739733	0.60	2.70	2.00	6.00
27	22	1	209910	741578	0.60	2.00	1.60	3.70
28	23	1	209900	741785	0.60	2.20	1.30	4.20
29	24	1	209900	741931	0.55	2.40	1.40	3.70
30	25	1	209894	742029	0.55	2.00	1.50	2.50
31	26	1	209895	742173	0.45	2.00	1.55	4.10
32	27	1	209864	741378	0.80	2.00	1.70	4.50
33	28	2	208711	739355	0.55	2.50	1.80	5.70
34	29	2	208703	739549	0.55	2.80	2.30	5.20

1	**2**	**3**	***4***	***5***	**6**	**7**	**8**	**9**
35	30	2	208718	738854	0.65	2.80	1.90	6.70
36	31	2	208718	739154	0.60	2.60	2.10	4.60
37	32	2	208694	738618	0.75	2.80	2.90	5.30
38	33	2	208678	738494	0.85	2.90	2.40	5.50
39	34	2	208691	738098	1.00	3.50	2.00	4.60
40	35	2	208662	737867	0.95	2.90	1.90	4.00
41	36	2	208682	737635	1.25	3.00	2.10	5.50
42	37	2	208701	737336	1.55	3.70	3.20	9.70
43	38	2	208693	737157	3.50	2.20		
44	39	3	207857	738303	0.70	2.30	1.80	3.70
45	40	3	207822	738134	1.80	2.70	3.20	5.40
46	41	3	207829	738051	5.60	2.60		
47	42	3	207910	738540	0.75	2.30	1.85	4.20
48	43	3	207847	738790	0.60	2.00	1.60	4.30
49	44	3	207922	741713	0.55	4.70	1.05	2.40
50	45	3	207932	741620	0.55	4.40	1.15	2.70
51	46	3	207911	741177	0.60	4.30	1.20	2.60
52	47	3	207906	741010	0.60	3.90	1.20	2.70
53	48	3	207913	740642	0.60	5.30	1.25	2.40
54	49	3	207920	740479	0.75	3.70	1.25	2.40
55	50	3	207887	740148	0.95	4.10		
56	51	3	207910	740313	1.00	4.80		
57	52	3	207891	739738	0.90	4.80		
58	53	3	207885	739843	0.95	4.30		
59	54	3	207861	739527	1.00	4.10		
60	55	3	207824	739357	1.15	4.30		
61	56	3	207795	739246	1.10	3.70		
62	57	3	207877	739090	1.20	4.30		
63	58	4	206138	740324	0.75	2.65		
64	59	4	206061	740257	0.95	2.40		
65	60	4	205973	740144	1.90	2.00	3.20	2.20
66	61	4	206236	740562	0.55	2.70	2.00	1.80
67	62	4	206156	740431	0.60	2.30		
68	63	1	209906	742564	0.45	2.00	1.55	4.30
69	64	1	209892	742429	0.50	2.00	1.50	4.60
70	65	1	210432	742566	0.45	2.50	2.20	4.50
71	66	1	210560	742973	0.50	2.40	2.20	4.40
72	67	4	206337	740649	0.65	2.20	2.20	2.00
73	68	4	206359	740886	0.65	2.70		
74	69	4	206535	741054	0.65	2.70		
75	70	4	206559	741253	0.45	4.00		
76	71	3	207801	741443	0.50	5.00	0.90	2.70
77	72	3	207855	741581	0.50	4.10	1.10	2.00
78	73	3	207858	738830	0.60	2.00	1.60	4.30
79	74	1	210070	741449	0.55	2.10	1.9 0	4.70
80	75	2	208774	742874	0.45	3.20	1.15	3.40
81	76	2	208760	743454	0.45	2.60	1.40	3.50

4. THE MECHANICAL PROPERTIES OF THE SUBSURFACE LAYERS IN THE INVESTIGATED AREA.

The key parameters to evaluate site effects analytically by 1D model for vertical incidence of shear wave using SHAKE program (Schnabel et al., 1972) are the S-wave velocity of the unconsolidated sediments, thickness of each layers, density and specific attenuation in different lithological units as well as S-wave and density of the reflector. Densities and specific attenuation in different lithological units are chosen on the base of literature sources (Borcherdt et al., 1989; McGarr et al., 1991; Theodulidis et al., 1996; Reinozo and Ordas, 1999; Pergalani et al., 2000 and many others). Recently, Pratt and Brocher (2006) used spectral decay in the shear-wave spectral ratio with respect to reference site amplification curves and estimated Q-values for shallow sedimentary deposits. They concluded that range of Q values is 10-40. This is just the range, which was used in this study.

In previous microzonation studies in Zevulun plain (Zaslavsky et al., 2006b, 2007a) limited data on sediment thickness and S-velocities available from a few refraction profiles and boreholes are used to constrain possible S-wave velocity structure via comparison with analytical transfer function. Table 2 summarizes the mechanical properties for the subsoil layers in investigated area.

Table 2. Mechanical properties of the materials used in the 1D model.

Lithological unit	**V_s** m/sec	**Density** g/cm^3	**Damping** %
Silt (Holocene)	160-180	1.5	3
Sand and sandy loam (Kurkar Gr., Pleistocene)	250-400	1.6-1.7	3
Gravels (Kurkar Gr., Pleistocene)	400-500	1.7	3
Calcareous sandstone (Kurkar Gr., Pleistocene) and clay (Pliocene)	600-650	1.8-1.9	2
	750-850	2	2
Sandy Limestone (Kurdani Fm., Pliocene-Pleistocene)	1100-1300	2	1
Gypsum and Limestone (Mavqi'im and Ziqlag Fms., Miocene)	1500	2.1	1
Chalk (Avedat Gr., Lower-Middle Eocene)	950-1050	2	1
Marl-chalk (Mount Scopus Gr., Senonian-Paleocene)	850-950	2	2
Limestone and dolomite (Judea Gr., Cenomanian-Turonian)	1900	2.2	

The parameters shown in table 2 have been tested at wells and a refraction profile located in the study area (Figure 2). Wells and the refraction profile, which we have, do not give the information about depth and velocity of the Judea Gr. Thus, we test and specify S-wave velocity structure for upper layers and calculate depth of the Top Judea for points measured at wells.

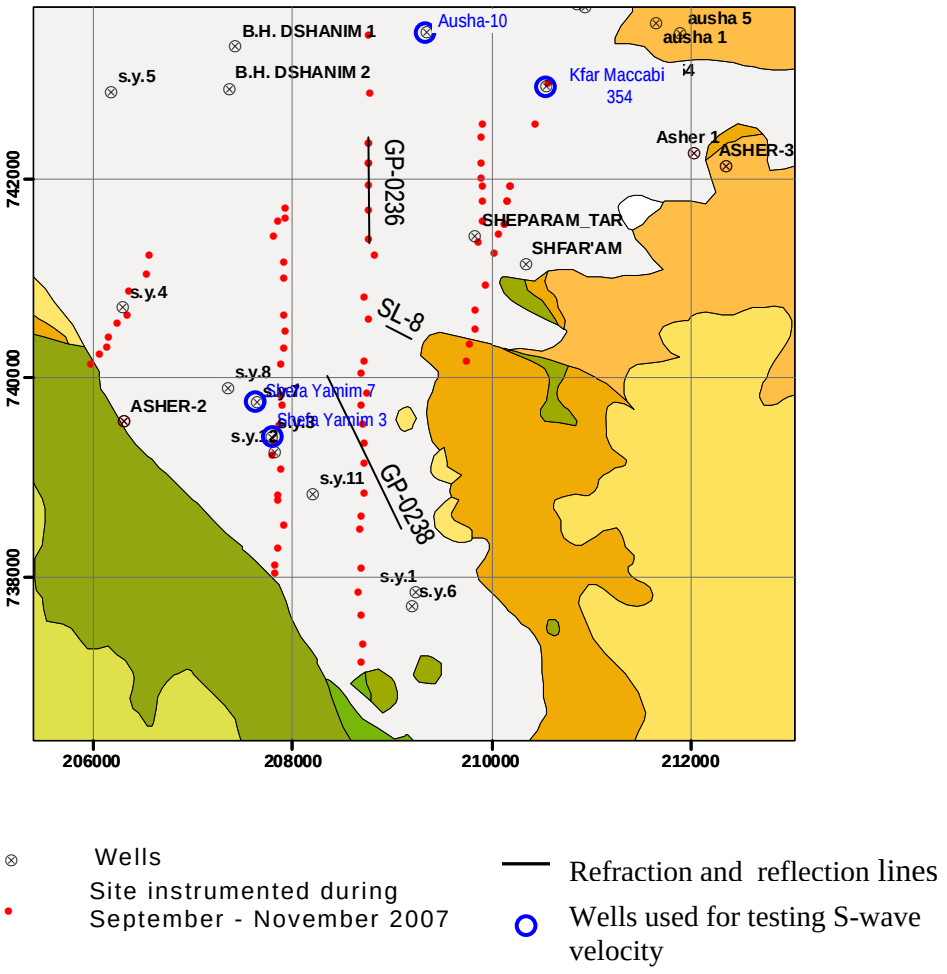

Figure 2. Location of wells, reflection and refraction line on Geological map.

Section of shear velocity Vs depth along refraction line SL-8 (Ezersky 2004) is shown in Figure 3. The lower layer of the section with Vs=1050 m/sec is correlated with chalk and chalky limestone of the Avedat Group (Adulam Member).

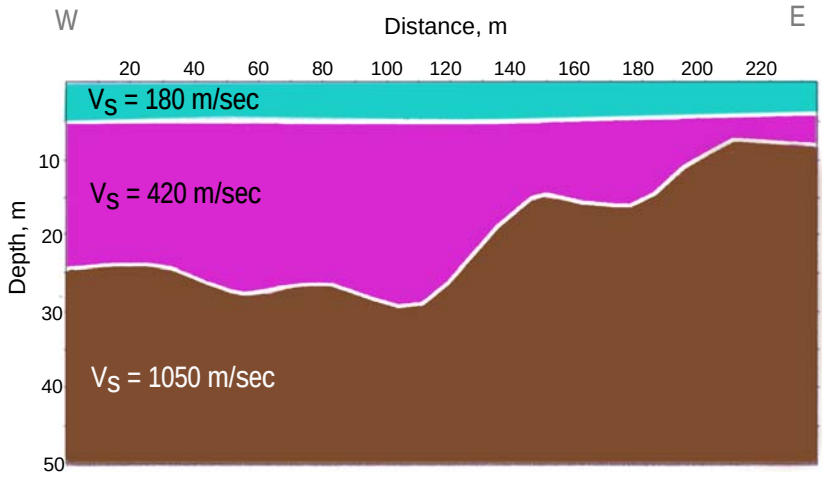

Figure 3. Vs-depth section along refraction line SL-8

For calibration we use four deepest wells in the area: Kfar Maccabi-354, Ausha-11, Shefa Yamim-3 and Shefa Yamim-7 (Figure 2).

Figure 4 shows a columnar section in Kfar Maccabi 354 well. The H/V spectral ratio obtained at measurement point 66, located at this well, is shown by the red line. Using S-wave velocities from Table 2 and borehole information shown in Table 3, we fit the Top Judea depth, the calculated theoretical transfer function (black line in Fig. 4) and compare it with the experimental spectral ratio.

Table 3. Soil column model for point 66 located at Kfar Maccabi-354 well.

Kfar Maccabi-354 well data		Soil column model	
Lithology	Thickness m	Thickness m	Vs m/sec
Silt & clay, gravel	45	45	350
Limestone	120	100	1300
Chalk and chalky limestone	-	435	1050
Limestone and dolomite	-		1900

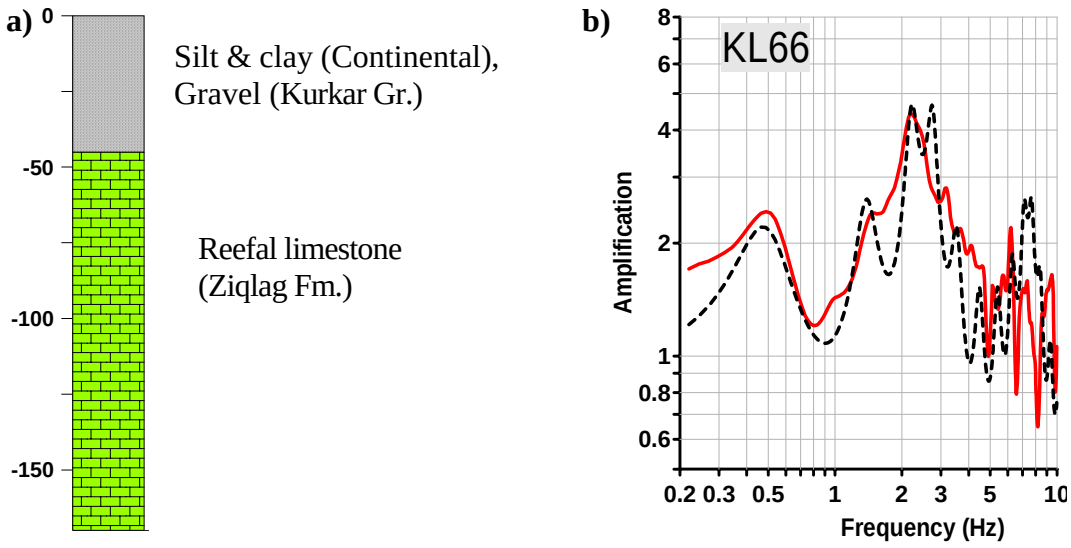

Figure 4. (a) - Lithological section of Kfar Maccabi-354 well and (b) - comparison between average H/V spectral ratio (red line) obtained at point 66 and analytical transfer function for Kfar Maccabi-354 well (black line).

Figure 5 shows a columnar section of Ausha 11 well. The H/V spectral ratio obtained at measurement point Q661, located at this well, is shown by the red line. Using S-wave velocity structure and borehole information shown in Table 4, we fit the Top Judea depth, the calculated theoretical transfer function (black line) and compare it with the experimental spectral ratio.

Table 4. Soil column model for point Q661 located at Ausha-11 well.

Ausha-11 well data		Soil column model	
Lithology	Thickness m	Thickness m	Vs m/sec
Silt & clay	15	15	200
Silt & clay, gravel	25	30	350
Sandy Limestone	10	10	1200
Limestone	100	100	1500
Chalk and chalky limestone	-	350	1050
Limestone and dolomite	-		1900

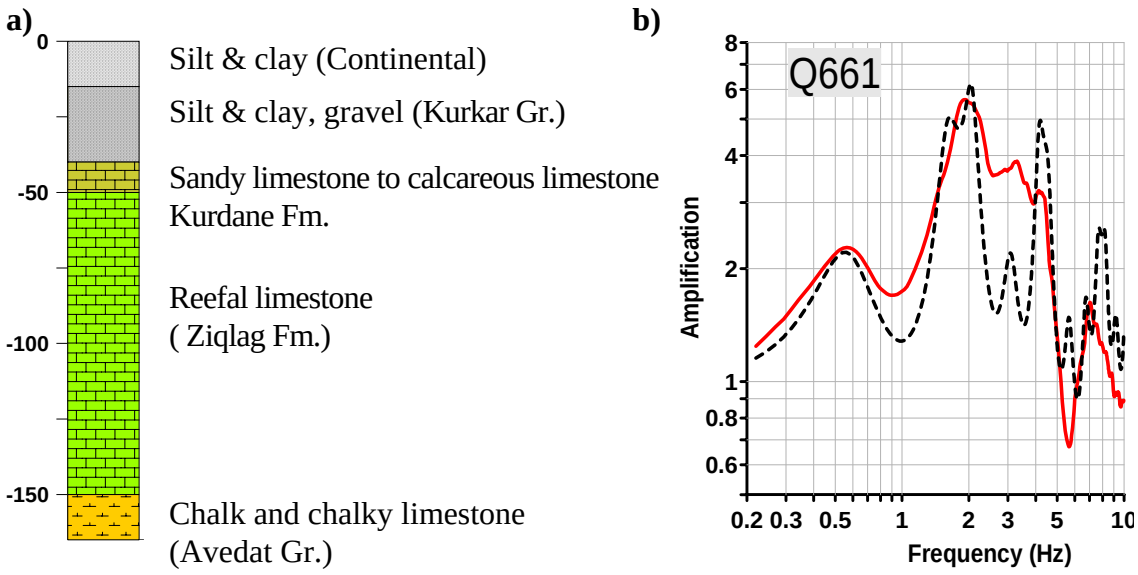

Figure 5. (a) - Lithological section of Ausha-11 well and (b) -comparison between average H/V spectral ratio (red line) obtained at point Q661 and analytical transfer function for Ausha-11 well (black line)

Figures 6 and 7 show columnar sections of the Shefa Yamim-3 and Shefa Yamim-7 wells. The H/V spectrals ratio obtained at measurement points KL55 and Q654, located at these wells, are shown in Fig. 6 and 7 by the red lines. Using S-wave velocity structure and borehole information shown in Tables 5 and 6 , we calculated the theoretical transfer function (black line in Fig. 6 and 7) and compared its with the experimental spectral ratios.

Table 5. Soil column model for point KL55 located at Shefa Yamim-3 well.

Shefa Yamim-3 well data		Soil column model	
Lithology	Thickness m	Thickness m	Vs m/sec
Silt & clay, gravel	80	75	370
Clays & marls	40	40	750
Limestone	60		1500
Chalk, conglomerate			

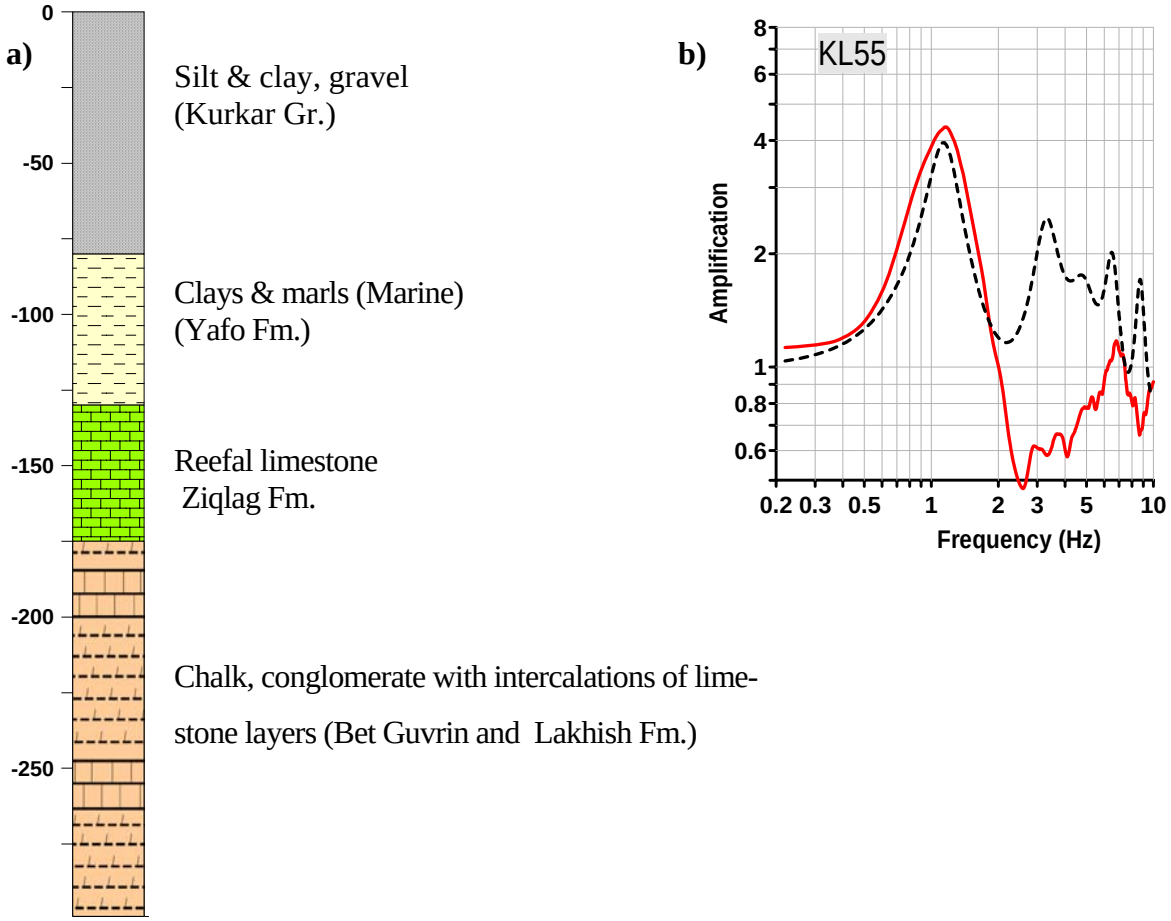

Figure 6. (a) - Lithological section of Shefa Yamim-3 well and (b) - comparison between average H/V spectral ratio (red line) obtained at point KL55 and analytical transfer function for Shefa Yamim-3 well (black line).

Table 6. Soil column model for point Q654 located at Shefa Yamim-7 well.

Shefa Yamim-7 well data		Soil column model	
Lithology	Thickness m	Thickness m	Vs m/sec
Silt & clay, gravel	80	80	360
Clays & marls	75	80	750
Limestone	20		1500
Chalk, conglomerate			

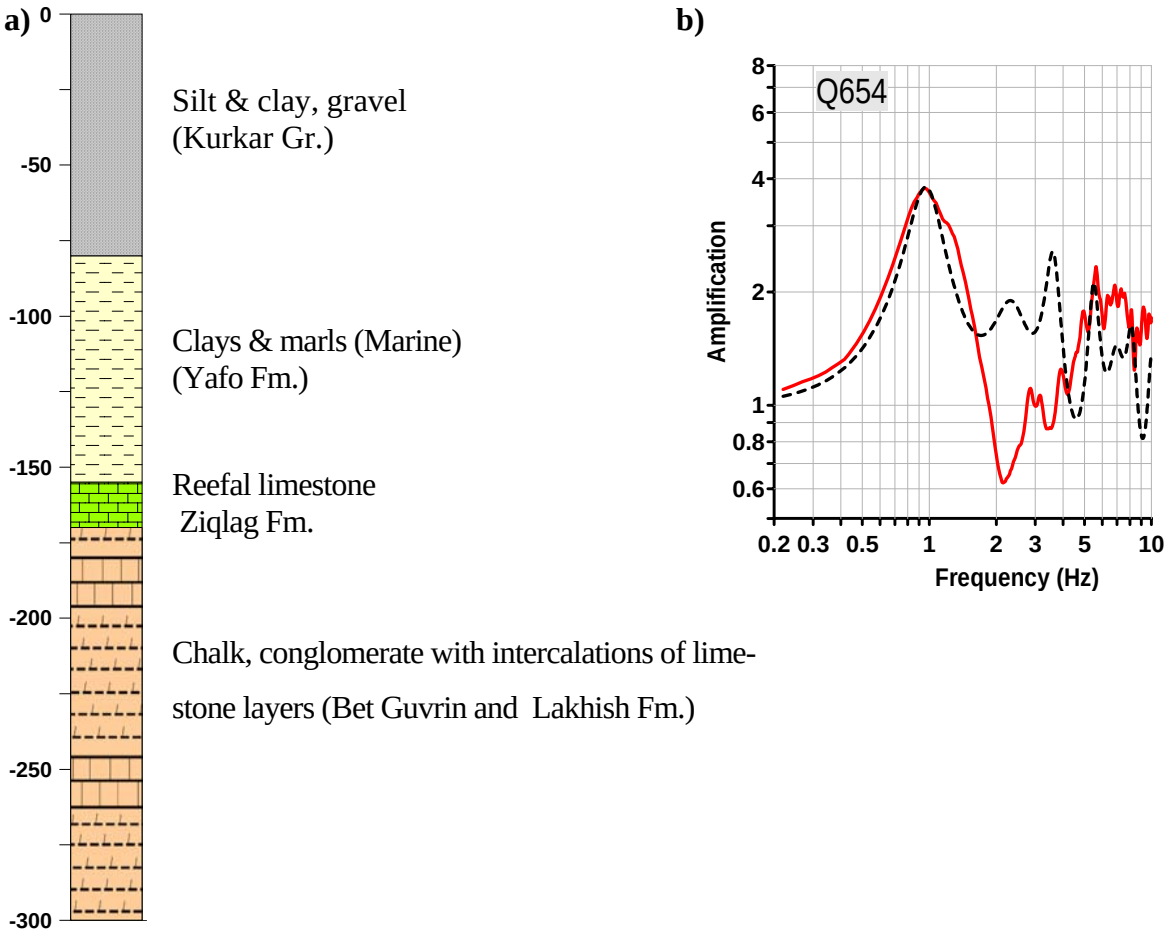

Figure 7. (a) - Lithological section of Shefa Yamim-7 well and (b) - comparison between average H/V spectral ratio (red line) obtained at point Q654 and analytical transfer function for Shefa Yamim-7 well (black line).

In all cases we obtain a good fit between the analytical transfer function and H/V spectral ratio received at points. It gives us the basis to consider, that S-wave velocities presented in Table 2 may be used in the investigated part of the Zevulun Plain.

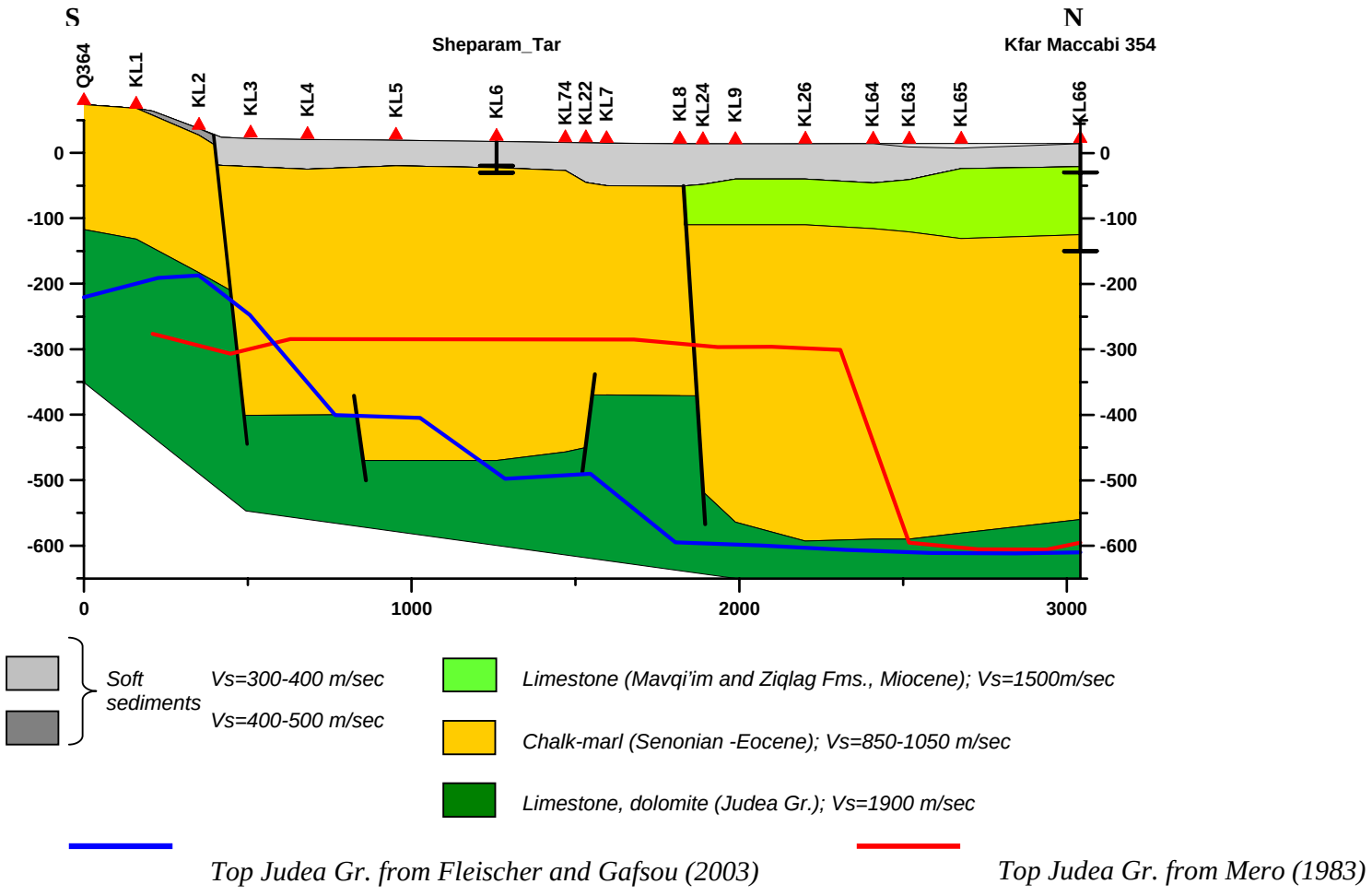

Figure 8. Schematic cross section along profile 1. For position see Fig.1

5. RECONSTRUCTION OF SUBSURFACE STRUCTURE ALONG PROFILES

5.1. Profile 1

As indicated in Fig. 1, profile 1 of 3.0 km long passes in S-N direction. Cross section along profile 1 reconstructed on the base of H/V spectral ratio analysis is shown in Fig. 8. H/V spectral ratios at points Q364 and KL1, located in the southern part of profile, show one resonance peak at frequencies 1.4 Hz and 1.3 Hz accordingly (Fig. 9). Depths of the reflector, which is associated with the Judea Gr., are 190 m and 200 m, respectively. Amplitude of the fundamental frequency (2-2.3 Hz) is formed by the impedance contrast between chalk and chalky limestone of Adulam Member (Avedat group) with Vs=1050 m/sec taken from refraction line SL-8 (Fig 3) and the limestone of the Judea Gr. with Vs=1900 m/sec. Both points are located on outcropping Adulam Member.

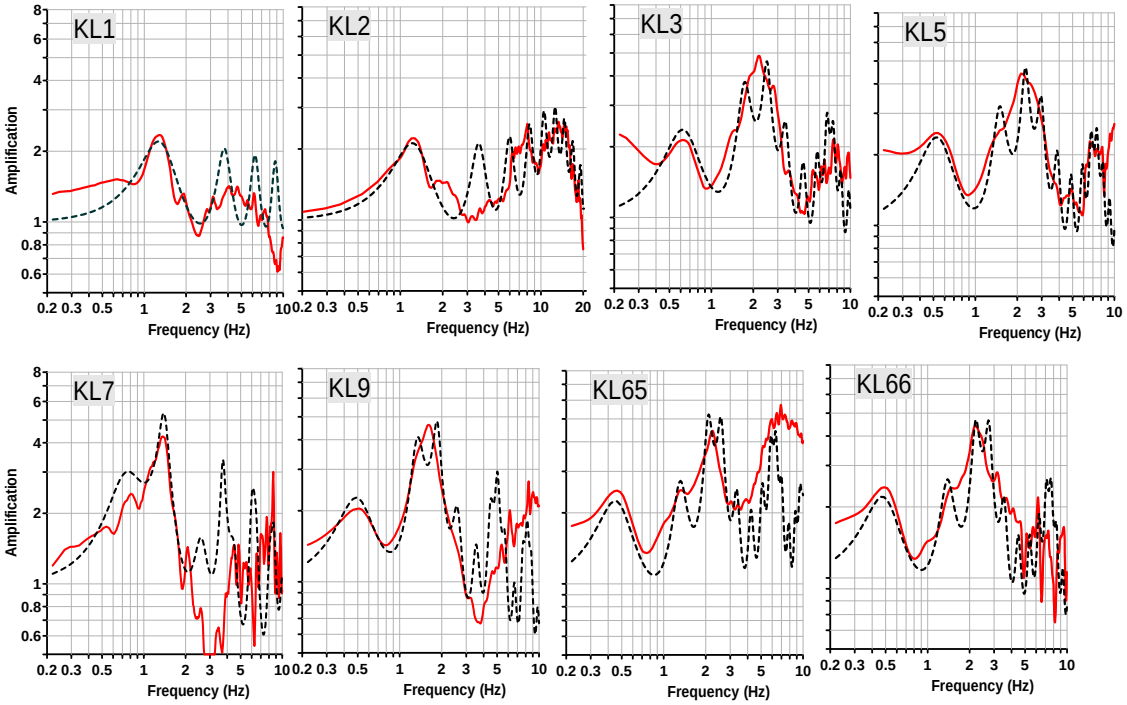

Figure 9. H/V spectral ratios (red line) and analytical transfer functions (black dashed line) in the profile 1

The second resonance peak, at frequency 8-13 Hz, appears at point KL2 (Fig. 9). It is associated with soft sediments over chalk and chalky limestone of Adulam Member (Avedat

groups). Thickness of soft sediments is less than 10 m. Fundamental frequency decreases to 1.2 Hz and Top Judea depth changes from 200 m to 220 m.

At points KL3 and KL4 (Fig. 9), both the fundamental and second frequencies decrease sharply to 0.65 Hz and 2.2 Hz, respectively. In accordance with the calculations, Top Judea depth changes from 220 m to 420 m and thickness of soft sediments increases to 40m. Sharp changes in the fundamental frequency between points KL2 and KL3 suggest the existence of a fault. Increase in the amplitude of the second peak from 2.3 (point KL2) to 4.5 (point KL3) may be interpreted as decrease in Vs of the upper layer from 500 m/sec to 350-400 m/sec. Despite the changes in Vs and thickness of the upper soft layer, amplitude of the fundamental frequency does not change. It may be explained by substantial increase in thickness of underlaying the soft sediments layer. It is also possible to assume, that the limestone of Ziqlag Formation is underlying the soft sediments. To test this hypothesis, in the course of modelling, we suggest an additional layer with Vs=1500 m/s below the upper layer. Setting thickness of this layer from 10 m to 60 m, we saw that analytical transfer functions does not change considerably. We repeat this procedure for every point of the segment of profile between KL3 and KL8 and get the similar results. Therefore, in the absense of any well data confirming the precence of the Ziqlag layer here, we do not show it in the cross section.

At points KL5, KL6 and an additional point KL74 (Fig. 9), the fundamental frequency decrease. Decrease in the fundamental frequency from 0.62 Hz to 0.5 Hz between points KL4 and KL5 (Fig. 8) corresponds to the increase in the reflector depth from 420 m to 500 m, which is probably accompanied by fault. The amplitude and frequency of the second peak do not change.

At points KL7 and KL8 (Fig. 9) the fundamental frequency increases to 0.75 Hz and second frequencies decreases to 1.4 Hz. In accordance with the calculations, reflector depth changes from 500 m to 375 m and thickness of soft sediments increases to 65 m. Sharp changes in the fundamental frequency between points KL74 and KL7 suggest the existence of fault. We note that there are two measuring sites only in this part of the profile. To be sure in correctness of our interpretation version, we carry out additional measurements at points located to the west from profile 1 (KL22, KL23, KL24, KL25, KL26). Though fundamental frequency at points KL22 and KL23 lower than at points KL7 and KL8, the tendency of reflector rising in S-N direction remains.

To understand the results of measurements received at point KL9, which is the last one in the profile, we have carried out measurements at well Kfar Maccabi 354 (KL66) and also at points KL65, KL63, KL64, KL26. Points KL63, KL64, KL26 are located to the west from the profile, due to technical reasons, it is possible to perform measurements only in this place.

Using S-wave velocity structure (Table 2) and the data of Kfar Maccabi 354 well, shown in Figure 4, we obtain a good fit between the analytical transfer function and H/V spectral ratio at point KL66. H/V spectral ratio at points KL65, KL63, KL64, KL26, KL9 practically do not differ from H/V spectral ratio at point KL66. Thus we utilize model of point KL66 for every point in this part of the profile. Decrease in the fundamental frequency from 0.75 Hz to 0.5 Hz between points KL7, KL8 and KL9 (Fig. 9) corresponds to increase in the reflector depth from 375 m to 570 m, which is probably accompanied by a fault.

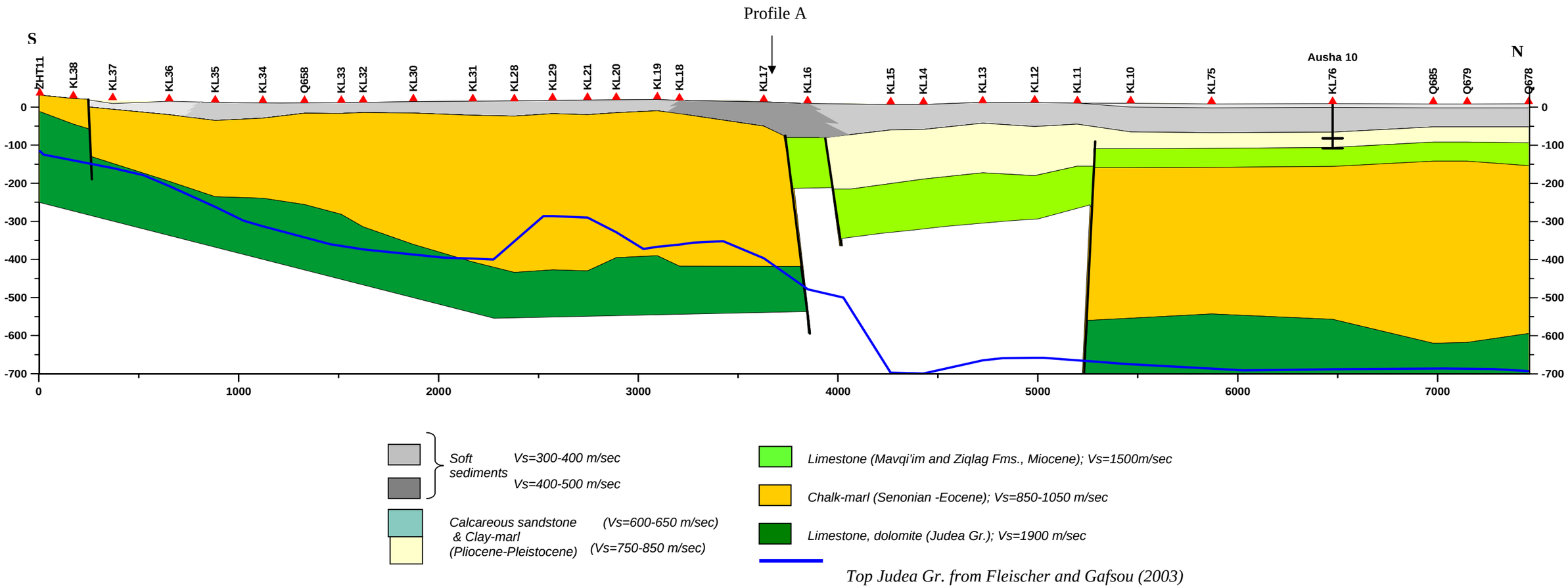

Figure 10. Schematic cross section along profile 2. For position see Fig.1

5.2. Profile 2

As indicated in Fig. 1, profile 2 of 7.5 km long passes in S-N direction. Cross section along profile 2 reconstructed on the base of H/V spectral ratio analysis is shown in Fig. 10.

H/V spectral ratio at points, located in the southern part of profile, shows one resonance peak at frequencies 5.7 Hz and 3.5 Hz (KL38) accordingly (Fig. 11). Depths of the reflector, which is associated with the Judea Gr., are 43 m and 67 m. Amplitude of the fundamental frequency is formed by the impedance contrast between marl-chalk of Mount Scopus Gr. Vs=950 m/sec and the limestone of the Judea Gr. (Vs=1900 m/sec).

Sharp decrease in the fundamental frequency from 3.5 Hz to 1.55 Hz occurs between points KL38 and KL37 (Fig. 11). This corresponds to the increase in the reflector depth from 67 m to 153 m respectively, which is probably accompanied by fault. The second resonance peak at frequency 3.5 Hz, appears at point KL37 (Fig. 11). It is associated with soft sediments over marl-chalk of Mount Scopus Gr. Point KL37 is distinguishable owing to high amplitude (9.7) of the second peak. Possible explanation is the presence of a layer with low velocity (Vs=160 m/sec) in the soft sediments.

At points KL36 and KL35 (Fig. 11), the fundamental frequencies decrease to 1.2 Hz and 1.0 Hz, respectively. In accordance with the calculations, Top Judea depth changes from 153 m (KL38) to 210 m (KL37) and to 250 m (KL36). Shift in the reflector depth by 50 and 40 m respectively can indicate presence of fault or heavy dip of the Top Judea.

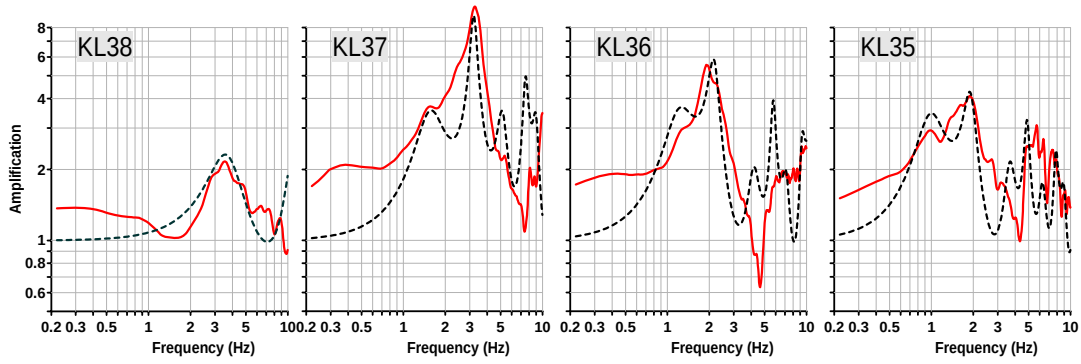

Figure 11. H/V spectral ratios (red line) and analytical transfer function (black dashed line) in the segment of profile 2 between points KL38 and KL35.

In the segment of profile 2 between points KL35 and KL33 (Fig. 12) the gradual decrease of fundamental frequency from 1.0 Hz to 0.85 Hz is observed. It matches the dipping of the Judea Gr. from 250 m down to 295 m.

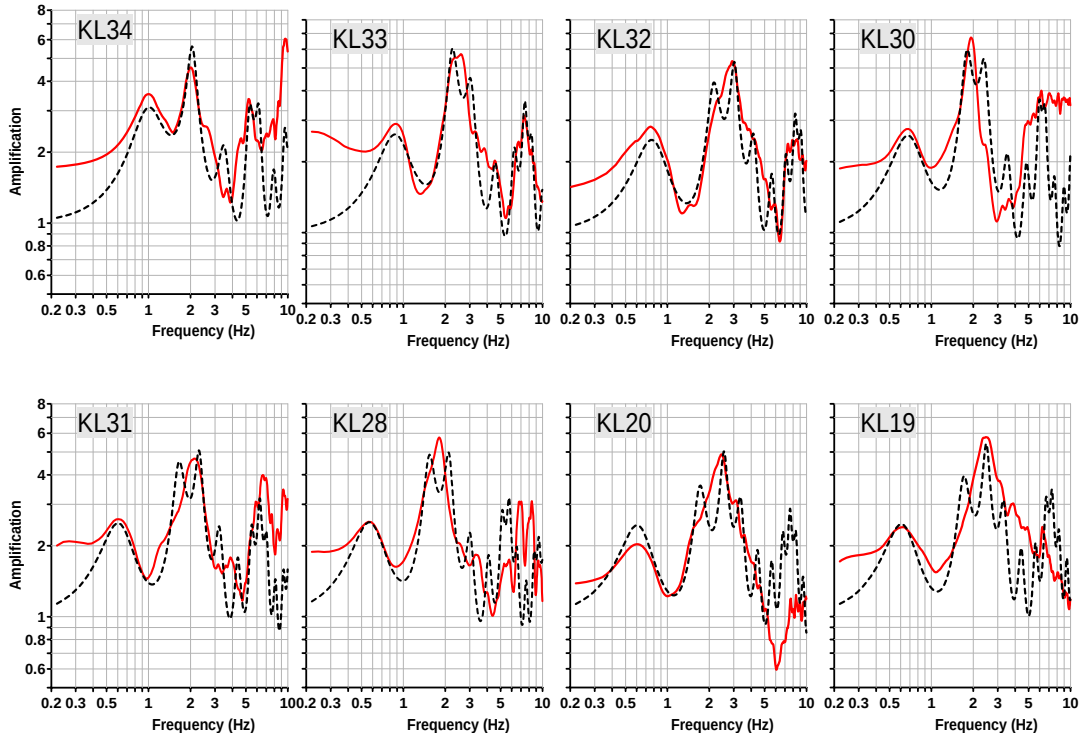

Figure 12. H/V spectral ratios (red line) and analytical transfer function (black dashed line) in the segment of profile 2 between points KL34 and KL19.

In the segment of profile 2 between points KL32 and KL28 (Fig. 11) a decrease of the fundamental frequency from 0.75 Hz to 0.55 Hz is observed. In accordance with the calculations, Top Judea at each point dips on 40-50 m in comparison with the previous one. In the segment of profile 2 between points KL28 and KL21, a change of the fundamental frequency is not observed and therefore the depth of the reflector does not change. At points KL20 and KL19 (Fig. 12), the fundamental frequency increases from 0.55 Hz to 0.6Hz and Top Judea rises by 40 m from 450 m to 410 m. Since reflector depth changes by 40-50 m, the measurements carried out along profile, are not sufficient for a substantiation of faults presence in the segment of profile 2 between points KL32 and KL19. Though, on seismic reflection profile GP-0238 (Medvedev, 2007), located near profile 2 (Fig 2), faults are detected, we do not have a sufficient base for identification of faults.

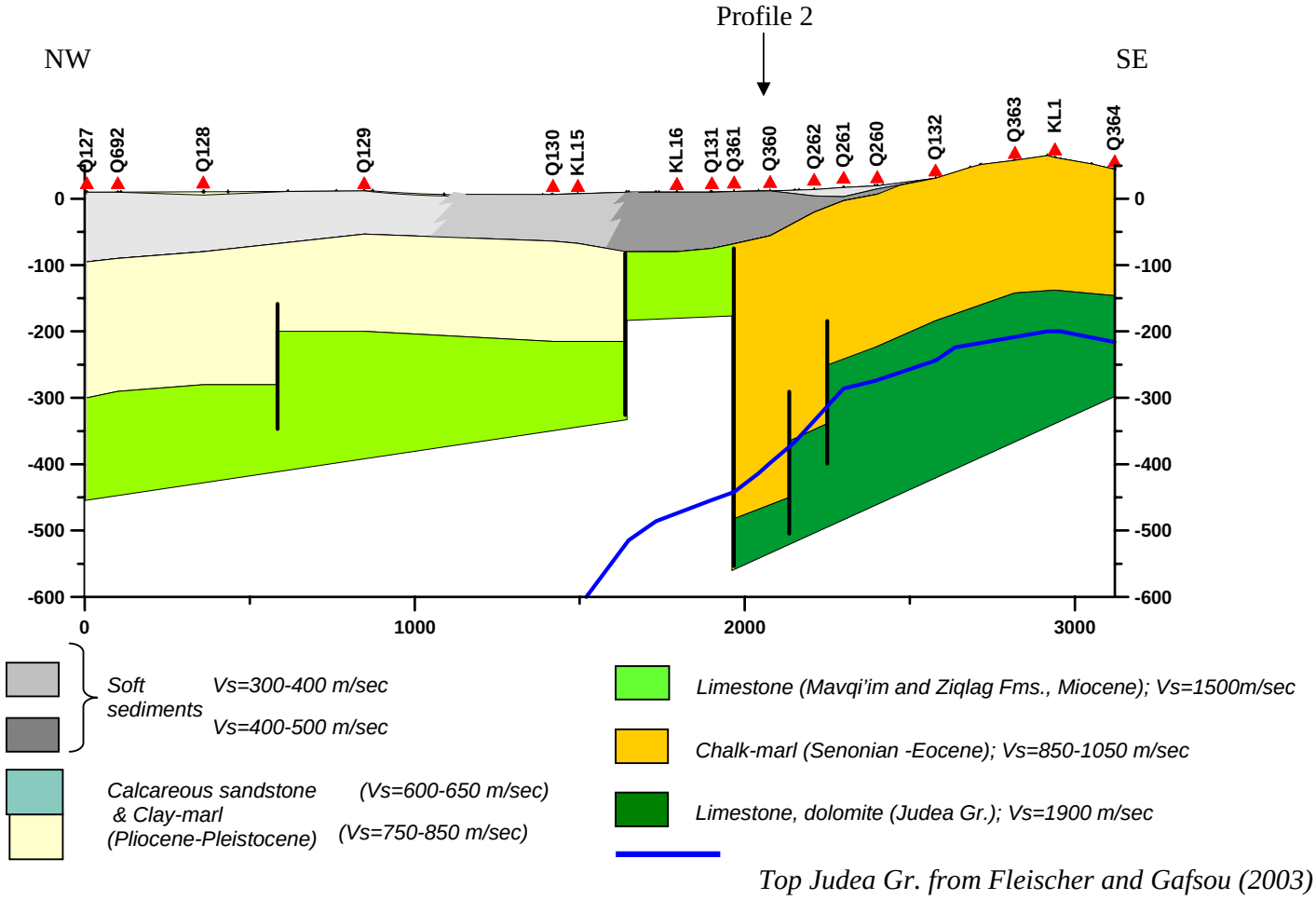

Figure 13. Schematic cross section along profile "A". For position see Fig.1

The second frequency in the segment of profile between points KL35 and KL19 changes in the range from 1.8 Hz to 2.5 Hz. As a result the thickness of the soft sediments varies from 30 m to 40 m.

For understanding of the geological structure in a segment of a profile 2 between points KL18 and KL11, we study profile 1 presented in Zaslavsky et al. (2006). New data have allowed specifying geological structures of a segment “A” on this profile. Profile “A” is presented in Figure 13 (in Figure 1 the location of a profile “A” is shown).

On Figure 14 pairs of points measured with a time interval of 2 years are shown. H/V spectral ratio at points KL17 and Q360 show two resonance peaks. The first one is associated with the Judea Gr. and the second peak is correlated with soft sediments over chalk and chalky limestone of Adulam Member (Avedat groups).

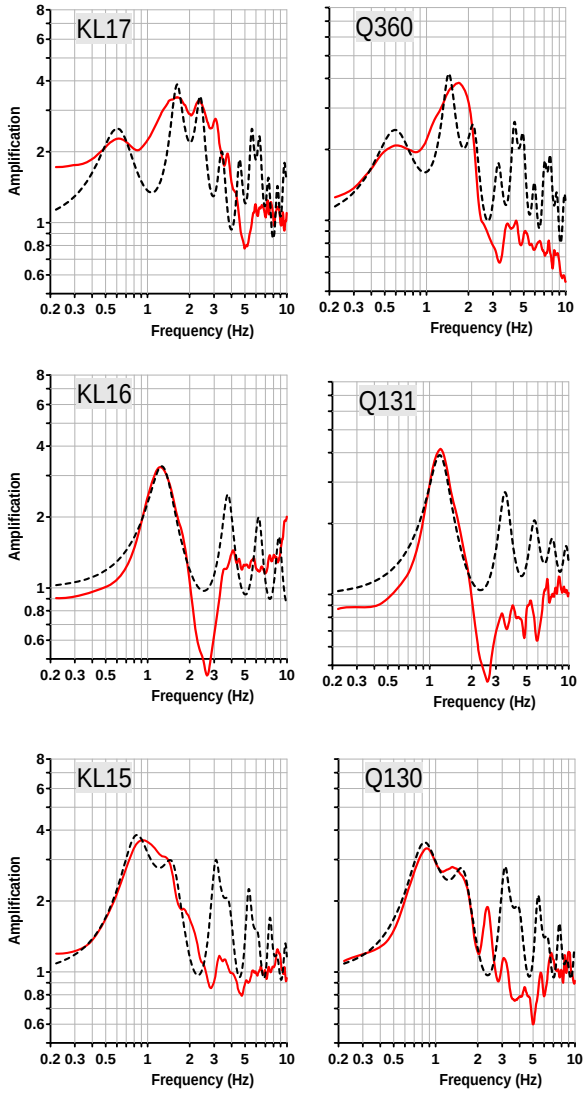

Figure 14. H/V spectral ratios (red line) and analytical transfer function (black dashed line) in the segment of profile 2 between points KL34 and KL19.

H/V spectral ratios at points KL16 and Q131show one resonance peak at frequency 1.2Hz (Fig. 14).Depth of the reflector associated with the Ziqlag Formation, is 90m. Amplitude of the fundamental frequency is formed by the impedance contrast between soft sediments over limestone of the Ziqlag Formation.

At points Q130 and KL15 (Fig. 14) fundamental frequency decreases to 0.85 Hz that corresponds to the dipping of Top Ziqlag Fm. to 220 m. Sharp changes in the fundamental frequency between points KL16 (Q131) and KL15 (Q130) suggest the existence of fault. The second resonance peak, at frequency 1.4 Hz, appears at points KL15 and Q130. It is associated with soft sediments over calcareous sandstone the Kurkar Gr. or clay/marl of Yafo Fm.

At points KL14-KL11 (Fig. 15) fundamental and second frequencies change slightly, that corresponds to insignificant variation of the depth of Top Ziqlag and Top Kurkar- Yafo.

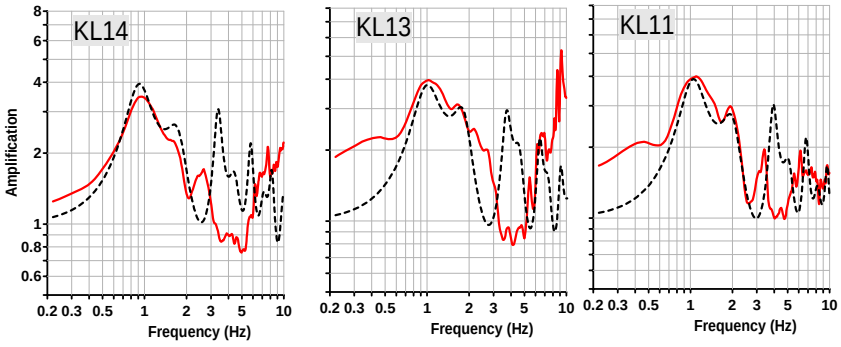

Figure 15. H/V spectral ratios (red line) and analytical transfer function (black dashed line) in the segment of profile 2 between points KL34 and KL19.

We note that all the points from KL15 to KL11 differ from points on profile 2 located south of point KL15, by both shape of the spectrum and H/V spectral ratio.

At point KL10 a change of the shape of spectrum and H/V spectral ratio is observed again. To understand the results of measurements obtained at point KL10, which is the last one in profile 2, we have carried out measurements at points KL75, KL76 and also have analysed new points measured at wells Ausha 10 (Q662) and Ausha 11 (Q661). Using S-wave velocity structure (Table 2) and the data of wells Ausha11and Ausha 10 shown in Figure 15 and 16, we obtain a good fit between the analytical transfer function and H/V spectral ratio at points Q661 and Q662.

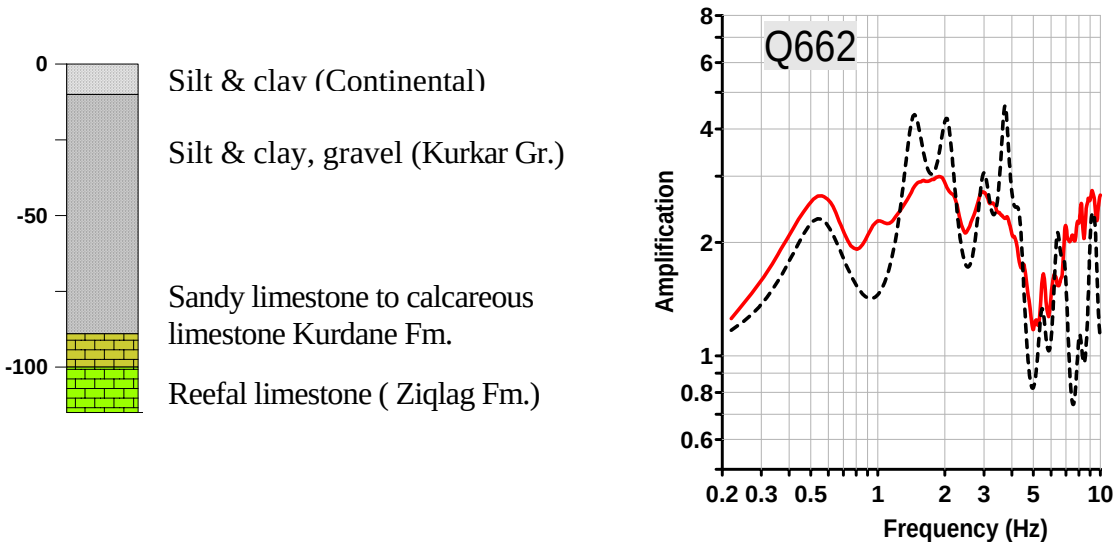

Figure 16. (a) - Lithological section of Ausha-10 well and (b) -comparison between average H/V spectral ratio (red line) obtained at point Q662 and analytical transfer function for Ausha-10 well (black line)

H/V spectral ratio at points KL75, KL76, and KL10 (Fig. 17) practically do not differ from H/V spectral ratio at point Q662. Thus we utilize model of point Q662 for points KL10, KL75 and KL76.

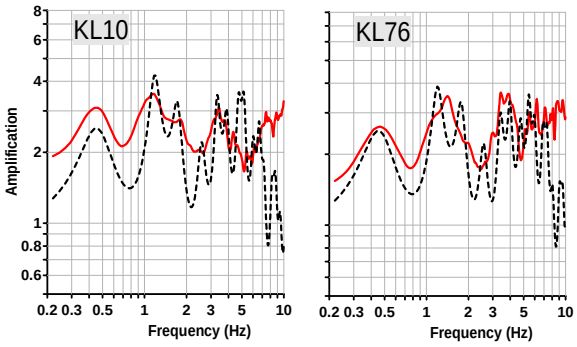

Figure 17. H/V spectral ratios (red line) and analytical transfer function (black dashed line) in the segment of profile 2 between points KL10 and KL76.

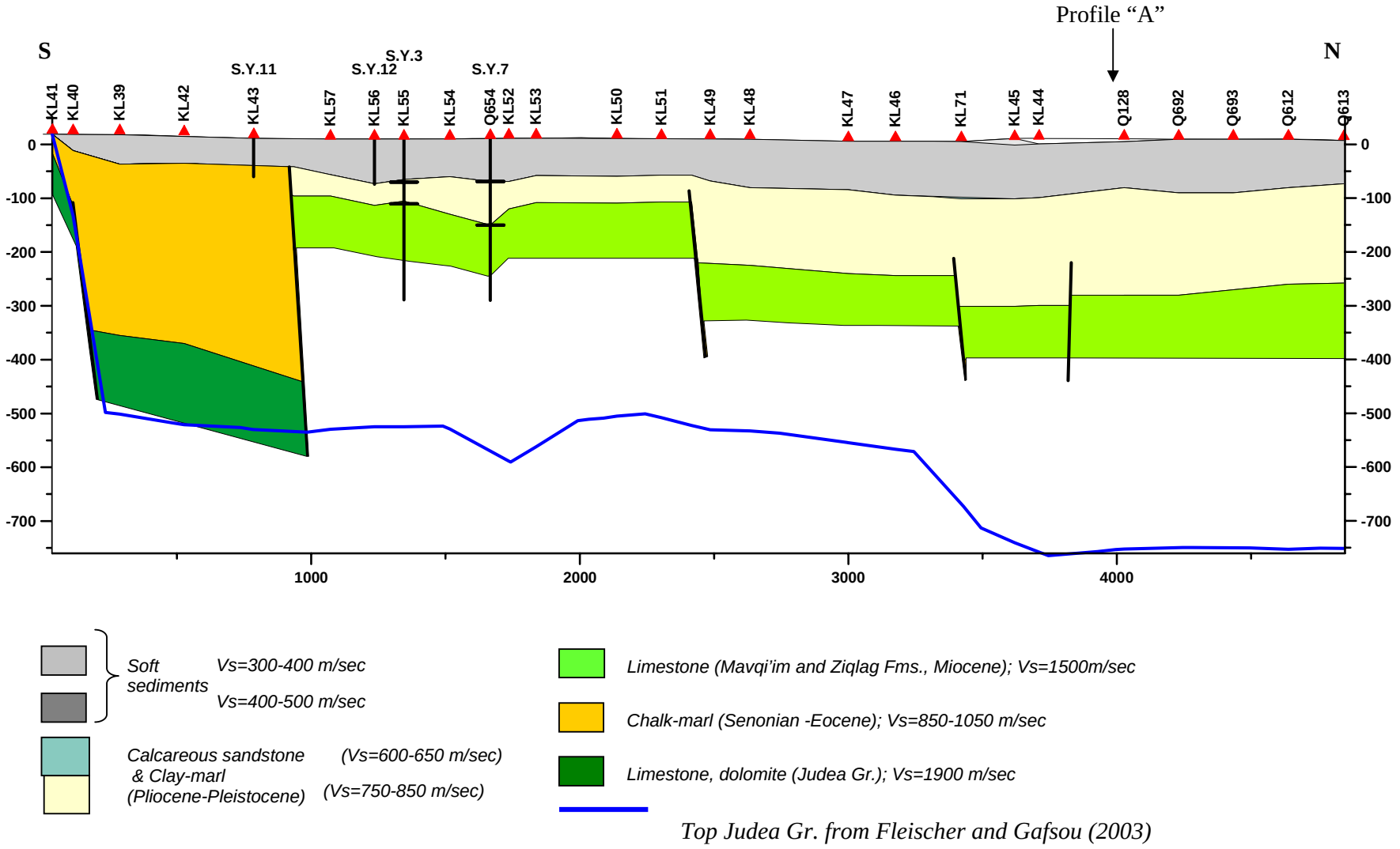

Figure 18. Schematic cross section along profile 3. For position see Fig.1

5.3. Profile 3

As indicated in Fig. 1, profile 3 of 4.82 km long passes in S-N direction. Cross section along profile 3 reconstructed on the base of H/V spectral ratio analysis is shown in Fig. 18.

At points KL41 and KL40 the fundamental frequency decreases from 5.6 Hz to 1.8 Hz. Depths of the reflector, which is associated with the Judea Gr., are 35 m and 155 m accordingly. Amplitude of the fundamental frequency is formed by the impedance contrast between marl-chalk of Mount Scopus Gr. (Vs=950 m/sec) and the limestone of the Judea Gr. (Vs=1900 m/sec). We consider that in segment of a profile 3, between points KL41 and KL40 located at a distance 80 m from each other, is observed high dip of Top Judea.

Sharp decrease in the fundamental frequency from 1.8 Hz to 0.7 Hz occurs between points KL40 and KL39 (Fig. 19). This corresponds to the increase in the reflector depth from 155 m to 375 m, respectively, which is probably accompanied by fault.

In the segment of profile 3 between points KL39 and KL43 (Fig. 19) the gradual decrease of fundamental frequency from 0.7 Hz to 0.6 Hz is observed. It matches the dipping of the Top Judea from 375 m down to 460 m.

H/V ratios at points KL40, KL39, KL42 and KL43 exhibit the second resonance peak associated with soft sediments over marl-chalk of Mount Scopus Gr.

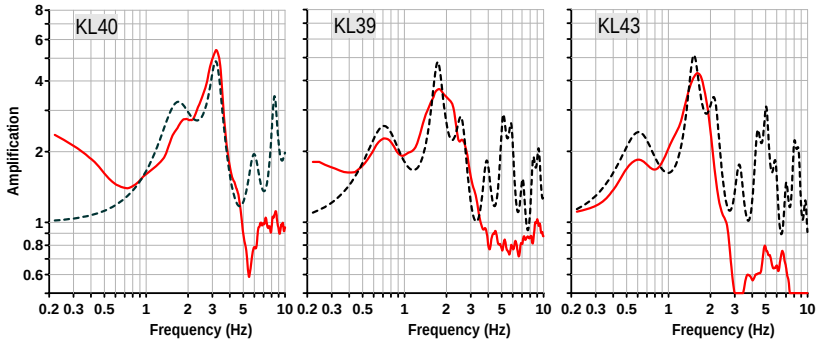

Figure 19. H/V spectral ratios (red line) and analytical transfer function (black dashed line) in the segment of profile 3 between points KL40 and KL43.

In the segment of profile 3 between points KL57 and KL51 (Fig. 20) shape of both spectrum and H/V spectral ratio are changes in comparison with previous points of the profile. Using S-wave velocity structure (Table 2) and the data of Shefa Yamim 3 and Shefa Yamim 7 wells, shown in Figures 6 and 7 respectively, we receive a good fit between the analytical

transfer function and H/V spectral ratio at points KL55 and Q654. H/V spectral ratio at the other points of the segment, practically do not differ from H/V spectral ratio at points KL57 and Q654. Thus we utilize model received at points KL57 and Q654 for the other points of the segment between points KL57 and KL51.

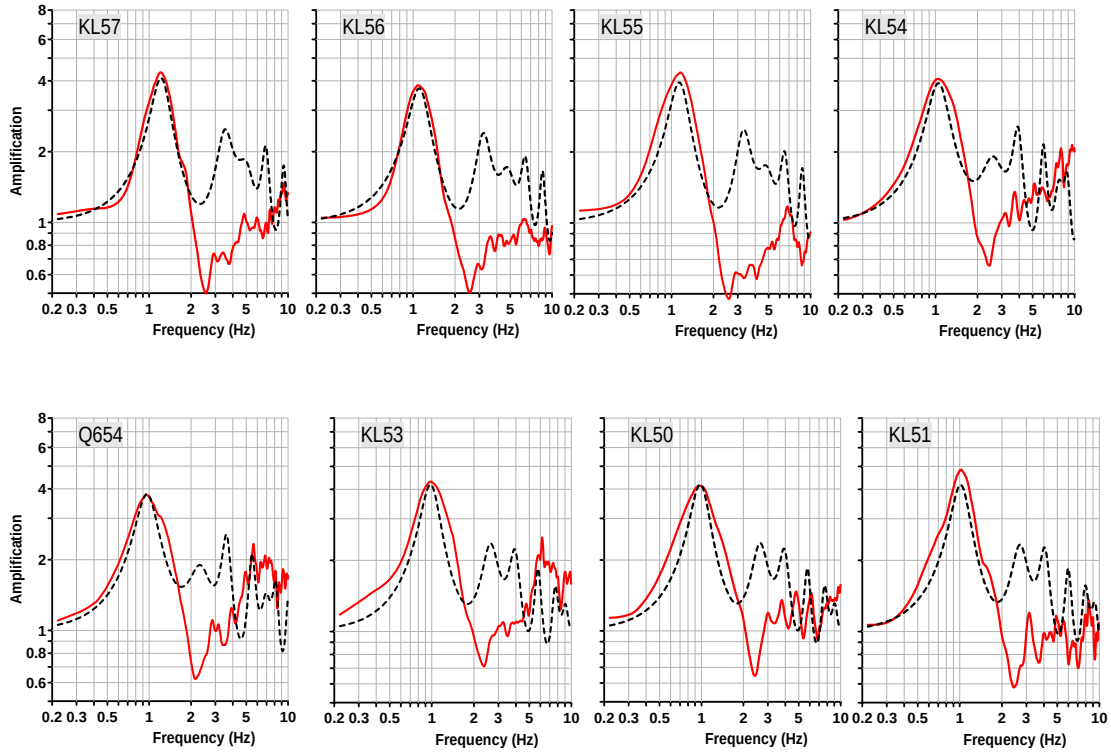

Figure 20. H/V spectral ratios (red line) and analytical transfer function (black dashed line) in the segment of profile 3 between points KL57 and KL51.

Sharp decrease in the fundamental frequency from 1.0 Hz to 0.75 Hz occurs between points KL51 and KL49. This corresponds to the increase in the reflector depth from 117 m to 220 m respectively, which is probably accompanied by a fault. The second resonance peak at frequency 1.25 Hz appears at point KL49 (Fig. 21). It is associated with an increase in the thickness of calcareous sandstone of the Kurkar Gr. or clay/marl of Yafo Fm. layers, which serve as a reflector for the soft sediments. At points KL48, KL47 and KL46 (Fig. 21) a decrease of the fundamental frequency to 0.6 Hz is observed. It matches the dipping of the reflector to 250 m.

At points KL71, KL45 and KL44 (Fig. 21) the fundamental frequency decreases to 0.5-0.55 Hz that corresponds to the dipping of Top Ziqlag Fm. to 310 m. Sharp change in the fundamental frequency between points KL46 and KL71 suggests the existence of a fault.

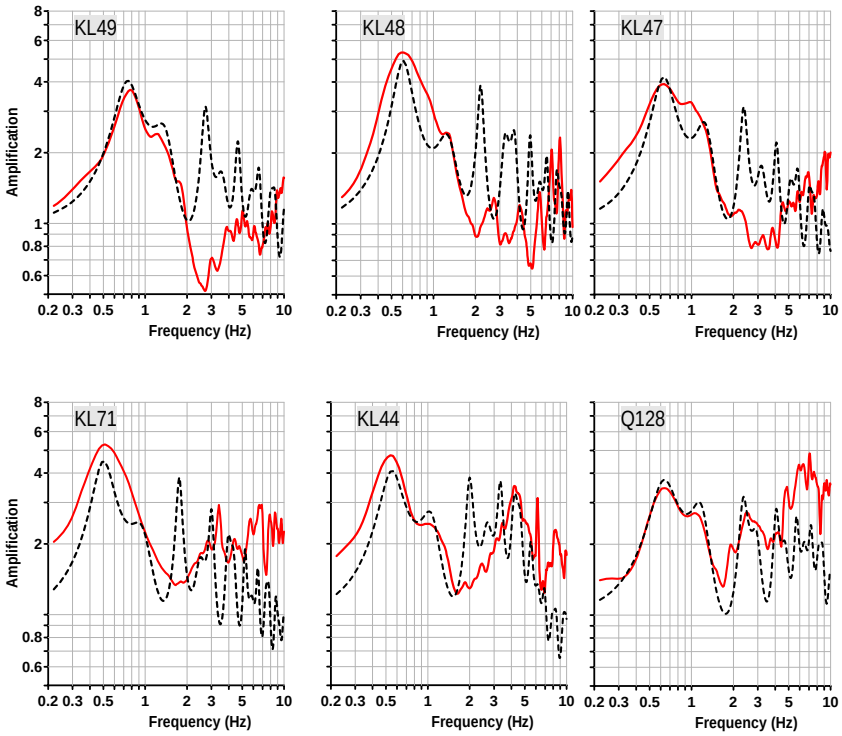

Figure 21. H/V spectral ratios (red line) and analytical transfer function (black dashed line) in the segment of profile 3 between points KL49 and KL128.

At point Q128 the fundamental frequency increases to 0.65 Hz. Though between points KL44 and Q128 a shift in the reflector depth is small, we suppose the presence of a fault in this place taking into account the fundamental frequency of 0.9 Hz obtained at point 129 in profile A (Fig. 13).

5.4. Profile 4

As indicated in Fig. 1, profile 4 of 1.4 km long passes in SW-NE direction. Cross section along profile 4 reconstructed on the base of H/V spectral ratio analysis is shown in Fig. 22.

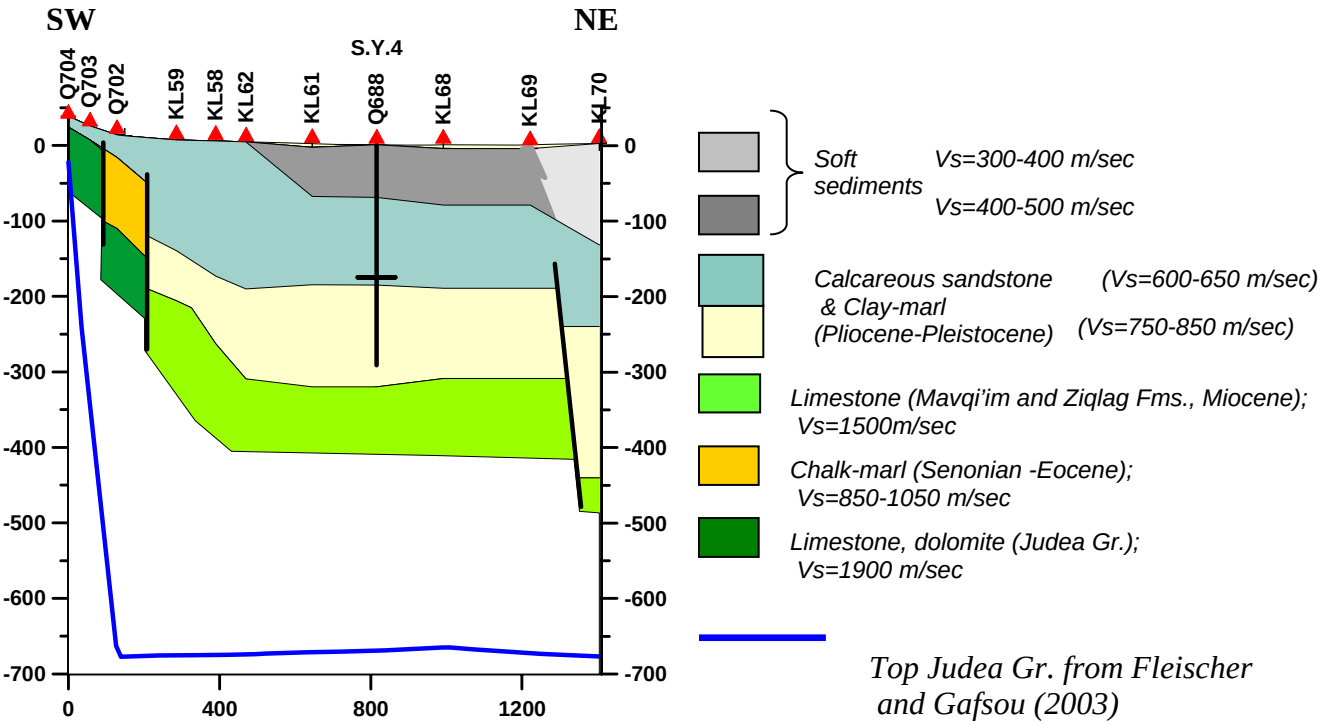

Figure 22. Schematic cross section along profile 4. For position see Fig.1

H/V spectral ratios at points located in the southwest part of profile show resonance peaks at frequencies 11.0 Hz for Q704 and 6.0 Hz for Q703 (see Fig. 23). Depths of the reflector, which are associated with the Judea Gr., are 14 m and 20 m accordingly. Amplitude of the fundamental frequency is formed by the impedance contrast between calcareous sandstone of the Kurkar Gr. (Vs=500-650 m/sec) and the limestone of the Judea Gr. (Vs=1900 m/sec). Sharp decrease in the fundamental frequency from 6.0 Hz to 2.25 Hz occurs between points Q703 and Q702 (Fig. 23). This corresponds to the increase in the reflector depth from 20 m to 125 m respectively, which is probably accompanied by a fault.

The second resonance peak at frequency 3.3 Hz appears at point Q702. It is associated with sand and calcareous sandstone over chalk and marl of the Avedat Gr. and/or Mount Scopus Gr.

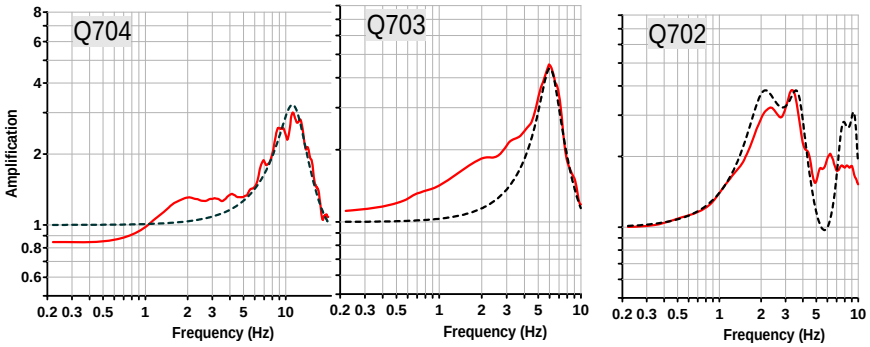

Figure 23. H/V spectral ratios (red line) and analytical transfer function (black dashed line) in the segment of profile 4 between points Q704 and Q702.

In the segment of profile 4 between points KL59 and KL69 (Fig. 24) we observe sharp decrease in the fundamental frequency and amplitude values and also change in the shape of both spectrum and H/V spectral ratio.

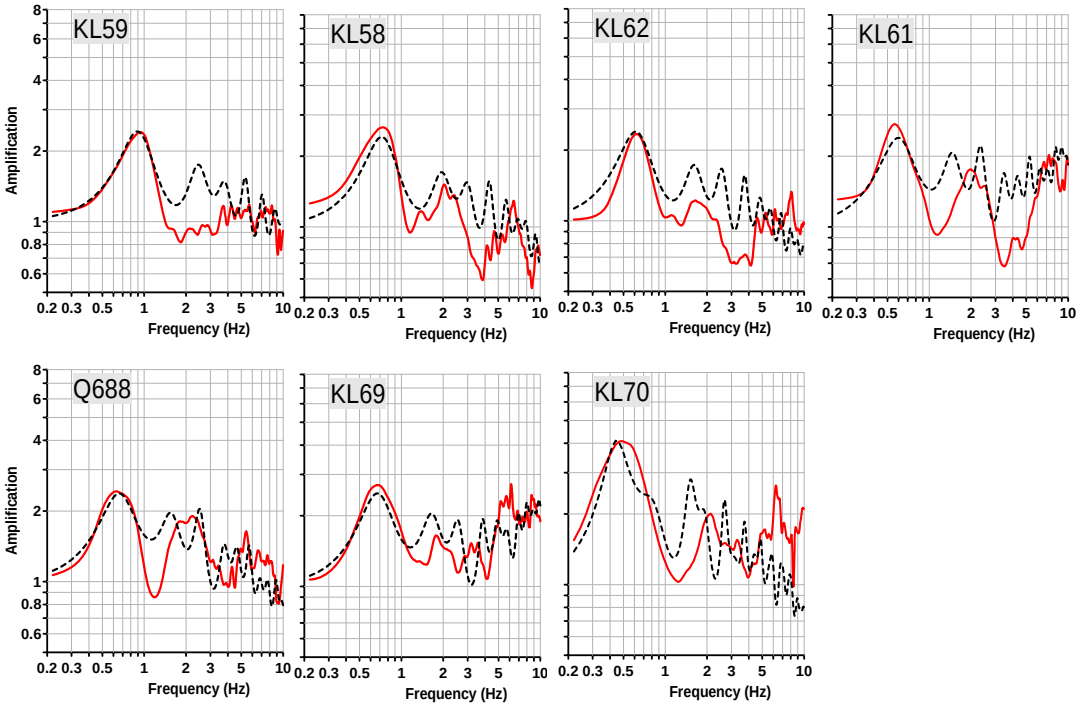

Figure 24. H/V spectral ratios (red line) and analytical transfer function (black dashed line) in the segment of profile 4 between points KL59 and KL70.

Using S-wave velocity structure (Table 2) and the data of Shefa Yamim 4 well, we fit the depth of reflector at the point Q688, located at this well, to reach a satisfactory agreement between the analytical transfer function and H/V spectral ratio. H/V spectral ratios at other points

of the described segment are similar to that at point Q688. Therefore, we assume a similar geological model for all points of this segment.

At points KL59, KL58 and KL62 (Fig. 24), the fundamental frequencies decrease from 0.9 Hz (KL59) to 0.75 Hz (KL58) and to 0.6 Hz (KL62). In accordance with the calculations, the depth of the Top Ziqlag Fm. changes from 210 m to 270 m and to 315 m, respectively. Change of the reflector depth by 50m and then 40 m can be explained by either the presence of faults or steep dip of the Top Ziqlag. Amplitude of the fundamental frequency is formed by the impedance contrast between calcareous sandstone of the Kurkar Gr. (Vs=600-650 m/sec), clay-marl of the Yafo Fm. (Vs=750-850 m/sec), and the limestone of the Ziqlag Fm. (Vs=1500 m/sec).

At points KL61, Q688 KL68 and KL69 (Fig. 24), the fundamental frequency practically does not change. At these points, the second resonance peak appears at frequency 2 Hz. It is associated with soft sediments (Vs=400-500 m/sec) over calcareous sandstone of the Kurkar Gr. (Vs=600-650 m/sec) together with clay-marl of the Yafo Fm. (Vs=750-850 m/sec).

At point KL70 (Fig. 24), the fundamental frequency decreases sharply to 0.45 Hz. In accordance with the calculations, Top Ziqlag depth changes from 320 m to 440 m and also the thickness of soft sediments increases. Sharp changes in the fundamental frequency between points KL69 and KL70 suggest the existence of fault. The point KL70 is last on profile 4. Additional measurements are necessary to verify presence of this fault.

6. CONCLUSIONS

The present study is focused on the ambient noise measurements along four profiles in the southern part of the Zevulun plain in order to reconstruct the subsurface structure. Total length of the profiles is 17.5 km and 76 sites were instrumented during the period September to November 2007. We have used in-situ measurements of shear wave velocity at shallow depth and detailed lithological information from boreholes to develop 1D multi-layer models for reconstruction of the subsurface structure. Our conclusions are based not only on investigation of 76 sites but also on the results obtained in the measurement campaigns in Qrayot, the Haifa bay area and along three profiles in the Zevulun plain (Zaslavsky et al., 2006c, 2007c).

We are aware, however, that due to non-uniqueness of the model solutions we cannot precisely determine the velocity and thickness for every layer in a multilayered structure.

Nevertheless, the exhaustive analysis of the H/V ratios, especially their shapes reflecting the variety of soil conditions, made possible to develop subsurface model that agrees well with both measurement results and geological information. Presence of the second peak in H/V ratio imposes additional restrictions on the subsurface model. Disagreement between the analytical model and H/V ratio causes the model to be revised.

The main conclusion can be summarized as follows:

- 1-D analytical models inferred from geological and geophysical information only may differ significantly from empirical assessments. Reliable estimations are those obtained by combining different empirical approaches, supplemented with geophysical and geological data.
- The ambient noise measurements in combination with Nakamura's method can be a powerful tool for exploration of sedimentary layers. In reconstructing the subsurface structure it is important to know the real value of the shear velocity for each layer of soil column. A detailed comparison of the analytical and experimental site response functions obtained from ambient noise measurements allowed establishing shear wave velocities of different lithological units and thickness of the sediments, i.e. reconstructing the subsurface structure.
- The ambient noise measurements allow identifying, and estimating vertical displacement of faults, which are defined as a discontinuity in the subsurface model and associated with:

  - a sharp shift in the fundamental frequency corresponding to a vertical displacement;

  - significant difference in all three characteristics of the H/V spectra, i.e. fundamental frequency, amplitude and shape corresponding to both vertical displacement and change in the velocity profile.
- Measurements of ambient noise solely along profiles in the area, where detailed microzonation study was not previously performed, may hamper interpretation of results and affect their fidelity and stability. Due to the lack of dense measurement grid, we fail to trace several faults inferred from microtremor measurements or other reasoning.

ACKNOWLEDGMENTS

We wish to express our thanks to Dr. A. Hofstetter for the fruitful discussion and constructive comments. Thank are also due to Y. Menahem for his assistance in preparing this report.

REFERENCES

Almagor G., Hall K.; 1980: *Morphology of the Continental Margin of Northern Israel and Southern Lebanon*. Israel Journal of Earth Sciences, Vol. 29, pp.245-252.

Almagor G.; 1993: *Continental Slope Processes off Northern Israel and Southern Lebanon and their Relation to Onshore Tectonics.* Marine Geology, Vol. 112, pp. 151-169.

Ambraseys, N.N., and Barazangi, B.; 1989: *The 1759 earthquake in the Bekaa Valley: implications for earthquake hazard assessment in the eastern Mediterranean region*. J. Geophys. Res. 94, 4007-4013.

Amiran, D.H.K., Arieh, E., Turcotte, T.; 1994: *Earthquakes in Israel and Adjacent Areas: Macroseismic Observations since 100 B.C.E*. Israel Exploration Journal, **2**, 261-305.

Arai, H., and Tokimatsu, K.; 2004: *S-wave profiling by inversion of microtremor H/V spectrum*. Bull. Seism. Soc. Am., 94, 53-63.

Bar Yossef, Y., Michaeli, A., Zah-Dvori, N., and Wolman, S., 2003: *Hydrological model (prediction) for testing producing scenarios in Naaman and Kurdani Aquifers*. Natural Resources Department LTD, Report NR/389/03.

Begin, Z. B.; 2005: *Destructive earthquakes in the Jordan Valley and the Dead Sea – their recurrence intervals and the probability of their occurrence.* Scientific Report GSI 12/05, The Geological Survey of Israel (in Hebrew with English summary), 32pp**.**

Borcherdt, R., Glassmoyer, G., Andrews, M. and Cranswick, E.; 1989: *Effect of site conditions on ground motion and damage,* Earthquake spectra, Special supplement, Armenia earthquake reconnaissance report: 23-42.

Delgado, J., López Casado, C., Giner, J., Estévez, A., Cuenca, A., and Molina, S.; 2000: *Microtremors as a exploration tool: application and limitations,* Pure and Applied Geophysics, 157, 1445-1462.

D'amico, V., Picozzi, M. and Albarello, D.; 2004: *Quick estimates of soft sediments thickness from ambient noise horizontal to vertical spectral ratios; a case study in southern Italy*, J. Earthq. Engineer., 8, 895-908.

Enomoto T., Kuriyama, T., Abeki, N., Iwatate, T., Navarro, M., and Nagumo, M.; 2000: *Study on microtremor characteristics based on simultaneous measurements between basement and surface using borehole*. In: Proc. of 12th World Conf. of Eart. Eng., Auckland.

Fäh, D., Kind, F., and Giardini, D.; 2003: *Inversion of local s-wave structures from average H/V ratios, and their use for the estimation of the site-effects*, J. Seismology **7**, 449-467.

Eytam Y., Ben-Avraham Z.; 1992: *Morphology and Sediments of the Inner Shelf of Northern Israel*. Israel Journal of Earth Sciences, 41, 27-44.

Fleischer, L., and Gafsou, R., 2003: *Top Judea Group – digital structural map of Israel.* The Geophysical Institute of Israel, Report 753/312/03.

Hinzen, K-G., Weber, B., and Scherbaum, F.; 2004: *On the resolution of H/V measurements to determine sediment thickness, a case study across a normal fault in the lower Rhine embayment, Germany*, J. Earthq. Engineer., 8 (6), 909-926.

Horike, M., Zhao, B., and Kawase, H.; 2001: *Comparison of site response characteristics inferred from microtremors and earthquake shear wave.* Bull. Seism. Soc. Am., 91, 1526-1536.

Ibs-von Seht, M., and Wohlenberg, J.; 1999: *Microtremor measurements used to map thickness of soft sediments*. Bull. Seism. Soc. Am., 89, 250-259

Kafri, U., and Ecker A., 1964: *Neogene and Quaternary subsurface geology and hydrogeology of the Zevulun Plain.* Geology Survey of Israel, Bull. No 37.

Konno, K., Ohmachi, T.; 1998: *Ground-motion characteristics estimated from spectral ratio between horizontal and vertical components of microtremors.* Bull. Seism. Soc. Am., **88**, 228-241.

Jenkins, M. G., and Watts, D. G., 1969. *Spectral analysis and its applications*. Holden-Day, San Francisco, 1969, 471 pp.

Kobayashi, K., Uetake, T., Mashimo, M., and Kobayashi, H.; 2000: *Estimation of deep underground velocity structures by inversion of spectral ratio of horizontal to vertical component in p-wave part of earthquake ground motion*. In: Proc. of 12th World Conference on Earthquake Engineering, Auckland, New Zealand, No. 2658.

Lachet, C., and Bard P.Y.; 1994: *Numerical and theoretical investigations on the possibilities and limitations of the Nakamura's technique*. J. Phys. Earth, *42*, 377-397.

McGarr, A., Celebi, M., Sembera, E., Noce, T. and Mueller, C.; 1991: Ground motion at the San Francisco international airport from the Loma Prieta earthquake, sequence, Bull. Seism. Soc. Am., 81, 1923-1944.

Mero, D., 1983. Subsurface geology of Western Galilee and Zevulun. Plain. TAHAL, Tel-Aviv, Internal Report No. 04/83/48: 36 pp.

Mucciarelli M.; 1998: *Reliability and applicability of Nakamura's technique using microtremors: an experimental approach*. J. of Earth. Eng, 4: 625-638.

Mucciarelli M., and Gallipoli, M. R., 2004. The HVSR technique from microtremor to strong motion: empirical and statistical considerations, in Proc. of 13th World Conference of Earthquake Engineering, Vancouver, B.C., Canada, Paper No. 45

Nakamura, Y.; 2000: *Clear identification of fundamental idea of Nakamura's technique and its applications.* In: Proc. of 12th World Conf. of Eart. Eng., CD-Rom, Auckland.

Parolai, S., Bormann, P. and Milkereit, C.; 2002: *New relationship between V_S, thickness of sediments, and resonance frequency calculated by the H/V ratio of seismic noise for the Cologne area (Germany)*, Bull. Seism. Soc. Am., *92 (*6), 2521-2527.

Parolai, S., and Galiano-Merino, J.J.; 2006: *Effect of transient seismic noise on estimates on H/V spectral ratios*. Bull. Seism. Soc. Am., *96, 228*-236.

Pergalani, F., Pomeo, R., Luzi, L., Petrini, V., Pugliese, A., and Sano, T.; 2000 : *Criteria for seimic microzoning of a large area in central Italy*, In: Proc. of 12th World Conf. of Earth. Eng., Auckland.

Reinoso, E., and Ordaz, M.; 1999: *Spectral amplification for Mexico City from free-field recordings*, Earthquake Spectra, Vol. *15 N*o. 2, p. 273-295.

Shapira, A. and Avirav, V.; 1995: *PS-SDA Operation Manual*. Technical Report IPRG, The Institute for Petroleum Research and Geophysics, Z1/567/79, 24pp.

Shapira A., Feldman, L., Zaslavsky, Y., and Malitzky, A.; 2001: *Application of a stochastic method for the development of earthquake damage scenarios: Eilat, Israel test case*. The Problems of Lithosphere Dynamics and Seismicity, Computational Seismology, 32, 58-73.

Zaslavsky, Y., Gitterman, Y., and Shapira, A., 1995: *Site response estimations using week motion measurements*, In: Proceedings of 5th Inter. Conf. on Seismic Zonation, Nice, 1713-1722.

Zaslavsky, Y., Shapira, A., Arzi, A.A.; 2000: *Amplification effects from earthquakes and ambient noise in Dead Sea Fault (Israel)*. Soil Dynamics and Earthquake Engineering, 20, 187-207.

Zaslavsky, Y., Shapira, A., and Leonov, J.; 2003: *Empirical evaluation of site effects by means of H/V spectral ratios at the locations of strong motion accelerometers in Israel*. J. of Earth. Eng., 7, 655-677.

Zaslavsky, Y., Gorstein, M., Aksinenko, T., Kalmanovich, M., Ataev, G., Giller, V., Dan, I., Giller, D., Perelman, N., Livshits, I., and Shvartsburg, A.; 2004: *Exploration of sedimentary layers and reconstruction of its subsurface structure for some areas of Israel by ambient vibration measurements.* In: Proceeding of XXIX General Assembly European Seismological Commission, Potsdam.

Zaslavsky, Y., Shapira, A., Gorstein, M., Kalmanovich, M., Giller, V., Perelman, N., Livshits, I., Giller D., and Dan, I.; 2005a: *Site response from ambient vibrations in the towns Lod and Ramle (Israel) and earthquake hazard assessment*. Bulletin of earthquake engineering, Vol. 3 No. 3, 355-381.

Zaslavsky, Y., Ataev, G., Kalmanovich, M., Gorstein, M., Mikenberg, M., Aksinenko, T., V. Giller, N. Perelman, I. Livshits, D. Giller, H. Dan, and. A. Shapira, 2005b. *Seismic hazard microzonation in Qiryat Shemona, northern Israe*l. In: Proceeding of International Conference of Earthquake Engineering in the 21st Century (EE-21C), CD-Rom, Skopje.

Zaslavsky, Y. Shapira, A. Gorstein, M. Aksinenko, T. Kalmanovich, M. Ataev, G. Giller, V. Perelman, N. Livshits, I. Giller, D. and Dan, H.; 2005c: *Expected site amplifications in the Coastal Plane of Israel*. In: Proc. of Inter. Conf. Earth. Eng. in the 21st Century (EE-21C), Skopje,.

Zaslavsky, Y., Gorstein, M., Aksinenko, T., Kalmanovich, M., Ataev, G., Giller, V., Dan, H., Giller, D., Perelman, N., Livshits, I and Shvartsburg, A.; 2006a: *Interpretation of microtremor H/V ratio in multilayered media: a study at Haifa bay, Israe*l. In: Proc. of First European Conf. on Earthquake Engineer. and Seism., CD-Rom, Geneva, Sept., 2006

Zaslavsky, Y., (Principal Investigator), 2006b. *Empirical determination of site local effect by ambient vibrations measurements for the earthquake hazard and risk assessment of Qrayot Haifa by areas*. Scientific Report No. 595/064/06.79 pp.

Zaslavsky, Y., Ataev, G., Gorstein, M., Kalmanovich, M., Hofstetter A., Perelman, N., Aksinenko, T., Giller, V., Dan, H., Giller, D., Livshits, I., Shvartsburg, A., and Shapira A.; 2007a: *Microzoning of site response parameters in the towns of Dimona and Bet Shean (Israel)*. Boll. di Geof. Teor. e. Appl., in press.

Zaslavsky, Y., Ataev, G., Gorstein, M., Kalmanovich, M., Perelman, N and Shapira A.; 2007b: *Assessment of site specific earthquake hazards in urban areas - A case study: The town of Afula, Israel, and neighbouring settlements.* Boll.di Geof.Teor ed Appl., in press.

Zhao, B., Horike, M., and Takeuchi Y.: 2000: *Analytical study on reliability of seismic site-specific characteristics estimated from microtremor measurements*. In: Proc. of 12th World Conf. Earth. Eng., Auckland.

יזרסקי מ., 2004. סקר רפרקציה סייסמית בעמק הזבולון, אזור קרית מוצקין. דו"ח מג"י 221/097/04. הוכן עבור ועדת ההיגוי להיערכות לטיפול ברעידות אדמה (משרד השיכון)

מדבדייב, ב., 2007. איתור העתקים חשודים כפעילים בעמק זבולון, דו"ח מג"י 381/265/07.